Universidade de Aveiro
Departamento de
Electrónica, Telecomunicações e Informática,
2019

Carlos Diogo
Mendonça Salgueiro

Técnicas de Equalização para MIMO massivo com amplificação não linear

Equalization Techniques for massive MIMO systems with non-linear amplification

Universidade de Aveiro
Departamento de Electrónica, Telecomunicações e Informática,
2019

Carlos Diogo Mendonça Salgueiro

Técnicas de Equalização para MIMO massivo com amplificação não linear

Equalization Techniques for massive MIMO systems with non-linear amplification

Dissertação apresentada à Universidade de Aveiro para cumprimento dos requesitos necessários à obtenção do grau de Mestre em Engenharia Electrónica e Telecomunicações, realizada sob a orientação científica de Professor Doutor Adão Paulo Soares da Silva, Professor Auxiliar do Departamento de Electrónica Telecomunicações e Informática da Universidade de Aveiro e da Doutora Sara Teodoro (co-orientador), investigadora no Instituto de Telecomunicações de Aveiro.

This work is supported by the European Regional Development Fund (FEDER), through the Competitiveness and Internationalization Operational Program (COMPETE 2020) of the Portugal 2020 framework, Regional OP Centro (CENTRO 2020), Regional OP Lisboa (LISBOA 14-20) and by FCT/MEC through national funds, under Project MASSIVE5G (PTDC/EEI-TEL/30588/2017)

o júri / the jury

presidente / president

Professor Doutor António Luís Jesus Teixeira

Professor Associado Com Agregação da Universidade de Aveiro (por delegação da Reitora da Universidade de Aveiro)

vogais / examiners committee

Professor Doutor Rui Miguel Henriques Dias Morgado Dinis

Professor Associado Com Agregação da Universidade Nova de Lisboa (Arguente Principal)

Professor Doutor Adão Paulo Soares da Silva

Professor Auxiliar da Universidade de Aveiro (orientador)

agradecimentos / acknowledgements

Em primerio lugar, um agradecimento aos meus pais e irmão, por todo o apoio e sacrificio, permitindo-me prosseguir com a minha formação.

Agradeço ao meu orientador, Professor Doutor Adão Silva, à minha co-orientadora, Doutora Sara Teodoro, por me acolherem neste projecto, pela ajuda e supervisão.

Ao Roberto Magueta do Instituto de Telecomunicações pela ajuda fundamental no desenvolvimento da plataforma de simulação.

À minha companheira Cristina, pelo carinho, motivação e ajuda na conclusão desta etapa.

A todos os amigos e colegas com que convivi ao longo destes anos, pela amizade e companheirismo.

À Universidade de Aveiro, ao Departamento de Eletrónica, Telecomunicacões e Informática e ao Instituto de Telecomunicacõespor fornecerem as condições necessárias de trabalho e aprendizagem.

Palavras-chave Ondas milimétricas, MIMO massivo, distorção não linear, amplificador de potência

Resumo

O surgimento de uma nova geração de comunicações móveis e a explosão de tráfego que advém da sua implementação apresenta grandes desafios. A banda de ondas milimétricas e o uso massivo de antenas são tecnologias que, combinadas, permitem atingir elevadas taxas de transmissão, funcionando em zonas do espectro electromagnético menos exploradas e com capacidade de alocação de dezenas de GHz para largura de banda.

Nesta dissertação foi considerado um sistema de MIMO massivo de ondas milimétricas usando uma arquitectura híbrida, i.e., o número de antenas para transmissão e recepção é menor que o número de cadeias de radiofrequência. Consequentemente, o pré-codificador e equalizadores devem ser projectados nos domínios digital e analógico. Na literatura, a maioria dos esquemas híbridos de *beamforming* são avaliados sem ter em conta os efeitos de não-linearidade da amplificação do sinal. No entanto, estes sistemas sofrem inevitavelmente de efeitos não lineares devido aos amplificadores de potência operarem em regiões não lineares. Os fortes efeitos das não-linearidades ao longo da cadeia de transmissão têm um efeito nefasto no desempenho do sistema e portanto o seu estudo e projecto de equalizadores que tenham em conta estes efeitos são de extrema importância.

Esta dissertação propõe um equalizador híbrido para sistemas baseados em ondas milimétricas para MIMO massivo com modulação SC-FDMA. Os terminais de utilizador possuem baixa complexidade, equipados apenas com pré-codificadores analógicos baseados no ângulo médio de partida, cada um com uma única cadeia de radiofrequência. Na estação base é projectado um equalizador iterativo híbrido analógico-digital com arquitectura completamente conectada de modo a eliminar a interferencia multi-utilizador e a distorção causada pela amplificação do sinal aquando da transmissão. O equalizador é optimizado minimizando a taxa de erro de bit, o que é equivalente a minimizar a taxa de erro quadrático médio. O impacto do limiar de saturação dos amplificadores no desempenho do sistema é analisado, e é demonstrado que o processo iterativo consegue eliminar de modo eficiente a interferência multi-utilizador e a distorção, melhorando o desempenho do sistema.

Keywords Milimeter wave, massive MIMO, non-linear distortion, power amplifier

Abstract

The dawn of the new generation of mobile communications and the traffic explosion that derives from its implementation pose great challenge. The milimeter wave band and the use of massive number of antennas are technologies which, when combined, allow the transmission of high data rate, functioning in zones of the electromagnetic spectrum that are less explored and with capability of allocation of dozens of GHz of bandwidth.

In this dissertation we consider a massive MIMO millimeter wave system employing a hybrid architecture, i.e., the number of transmit and receive antennas are lower than the number of radio frequency chains. As consequence, the precoder and equalizers should be designed in both digital and analog domains. In the literature, most of the proposed hybrid beamforming schemes were evaluated without considering the effects of nonlinear amplifications. However, these systems face non-avoidable nonlinear effects due to power amplifiers functioning in nonlinear regions. The strong nonlinear effects throughout the transmission chain will have a negative impact on the overall system performance and thus its study and the design of equalizers that take into account these effects are of paramount importance.

This dissertation proposes a hybrid iterative equalizer for massive MIMO millimeter wave SC-FDMA systems. The user terminals have low complexity, just equipped with analog precoders based on average angle of departure, each with a single radio frequency chain. At the base station it is designed an hybrid analog-digital iterative equalizer with fully connected architecture in order to eliminate both the multi-user interference and the nonlinear distortion caused by signal amplification during the transmission. The equalizer is optimized by minimizing the bit error rate, which is equivalent to minimize the mean square error rate. The impact of the saturation threshold of the amplifiers in the system performance is analysed, and it is demonstrated that the iterative process can efficiently remove the multi-user interference and the distortion, improving the overall system performance.

Contents

Contents i

List of Figures vii

List of Tables ix

1 Introduction 1

1.1 History . . . 1

1.2 Future system 5G and beyond . . . 5

1.3 Motivation and objectives . . . 10

1.4 Document structure . . . 11

1.5 Notations . . . 12

2 State of the art 13

2.1 Modulation schemes . . . 13

2.1.1 Orthogonal frequency division multiplexing . . . 14

OFDM architecture . . . 15

OFDMA . . . 16

2.1.2 SC-FDMA system . . . 17

2.2 Multiple antenna systems . . . 19

2.2.1 MIMO techniques . . . 20

2.3 Power amplifier . . . 22

2.4 Non-linear distortion . . . 26

2.5 Interference cancelation . . . 26

2.5.1 Concept of IB-DFE . . . 27

3 Millimeter wave systems and Massive MIMO 31

3.1 Millimeter wave communications . . . 31

3.1.1 Spectrum . . . 33

3.1.2 Millimeter wave propagation . . . 34

3.1.3 Milimeter-wave mobile broadband network infrastructure 35
3.1.4 Massive MIMO with millimeter wave 36
3.1.5 Beamforming 37
3.2 Massive MIMO with Hybrid analog and digital BF 39
3.2.1 Hybrid BF structure 40
3.3 MIMO precoding and combining in mmWave 41
3.3.1 Hybrid analog/digital precoding and combining 42
3.3.2 Precoding and combining with low resolution ADC 43

4 Proposed receiver structure for massive MIMO mmWave systems 45
4.1 System characterization 46
4.1.1 Channel model 46
4.1.2 Transmitter model 47
4.1.3 Receiver model 49
4.2 Receiver description 50
4.3 Results 53
4.3.1 Scenario A 55
4.3.2 Scenario B 59

5 Conclusion and future work 63
5.0.1 Conclusions 63
5.0.2 Future work 64

Bibliography 67

List of Acronyms

1G	First generation of mobile technologies
2G	Second generation of mobile technologies
3G	Third generation of mobile technologies
3GPP	3rd Generation Partnership Project
4G	Fourth generation of mobile technologies
5G	Fifth generation of mobile technologies
5G-NR	5G-New Radio
ADC	Analog-to-digital converter
AMPS	Advanced Mobile Phone System
AoA	Angle of arrival
AoD	Angle of departure
BF	Beamforming
CP	Cyclic-prefix
D2D	Device-to-device
DAC	Digital-to-analog converter
DFT	Discrete Fourier transform
EDGE	Enhanced Data Rates for GSM Evolution
EE-SE	Energy efficiency versus spectrum efficiency
EGC	Equal gain combining
ETSI	European Telecommunications Standards Institute
FDMA	Frequency division multiple access
FFT	Fast Fourier transform
GPRS	General Packet Radio Service

GSM	Global System for Mobile communications
IB-DFE	Iterative block-decision feedback equalization
ICI	Inter-carrier interference
IoT	Internet of things
ISI	Inter-symbol interference
ITU	International Telecommunications Union
KKT	Karush-Kuhn-Tucker
LOS	Line of sight
M2M	Machine to machine
MIMO	Multiple input - multiple output
MMB	Millimeter wave mobile broadband
MMS	Multimedia messaging service
mmWave	Millimeter wave
MMSE	Minimum mean square error
MRC	Maximal ratio combining
NLD	Non-linear distortion
NLOS	Non-line of sight
NMT	Nordic Mobile Telephony
OFDM	Orthogonal frequency division multiplexing
OFDMA	Orthogonal frequency division multiple access
PA	Power amplifier
PANC	PA non-linearity cancellation
PAPR	Peak-to-average power ratio
PIC	Paralel interference cancellation
RAN	Radio access network
RAT	Radio access technologies

RF	Radio frequency
SC-FDMA	Single carrier - (orthogonal) frequency division multiple access
SE	Spectrum efficiency
SIC	Successive interference cancellation
SISO	Single input - single output
SMS	Short message service
SNR	Signal to noise ratio
SSB	Synchronization signal block
SSPA	Solid-state power amplifier
TACS	Total Access Communication System
TDMA	Time division multiple access
TWTA	Travelling-wave tube amplifier
UE	User equipment
ULA	Uniform linear array
UTRA	Universal Terrestrial Radio Access
WAP	Wireless Application Protocol
WCDMA	Wideband code division multiple access
WLAN	Wireless local area network
ZF	Zero forcing

List of Figures

1.1 Examples of pre-radio telecommunication systems 2
1.2 The telegraph system 2
1.3 Bell's MTS system, accommodated in the trunk of an automobile [6] 3
1.4 Evolution of wireless communications 4
1.5 Annual global technology growth [10] 5
1.6 Technical directions of wireless evolution [11] 6
1.7 Heterogeneous networks, present and future 7
1.8 Annual global technology subscriptions forecast 2019-2023 [10] 8
1.9 Global mobile data traffic in Exabytes per month [14] 9
1.10 Performance requirements for 5G 10

2.1 Basic principle of FDMA 14
2.2 Multicarrier arrangement in OFDM 14
2.3 Transceiver structure of a typical OFDM system 15
2.4 Cyclic-prefix method to overcome ISI 15
2.5 OFDM and OFDMA allocation schemes [24] 16
2.6 Transceiver structure of a typical SC-FDMA system 17
2.7 Transmission methods of OFDM and SC-FDMA - comparison [24] 18
2.8 Single or multiple antenna arrangements 19
2.9 Generic representation of MIMO system 20
2.10 MIMO techniques [32] 21
2.11 Amplifiers classes and efficiency [36] 23
2.12 Linear PA behavior with saturation [37] 23
2.13 Block diagram of non-linear amplification 25
2.14 Output amplitude vs Input amplitude for Rapp model of PA [42] 25
2.15 Linear PA behavior with applied predistortion [43] 27
2.16 Iterative receiver structure based on IB-DFE SIC approach [46] 28
2.17 Iterative receiver structure based on IB-DFE PIC approach [46] 28

3.1 Examples of wearable devices around user [47] 32
3.2 Overview of vehicular networks [47] 32
3.3 Current spectrum allocation 33
3.4 Atmospheric and molecular absorption at mmWave frequencies [47] 34
3.5 Hybrid MMB+4G - architecture and system [52] 36
3.6 Antenna arrays for massive MIMO [54] 37
3.7 Beamforming and beam steering using MIMO [56] 38
3.8 BF with multi level sectorization [57] 38
3.9 $N \times M$ hybrid BF structure [15] 40
3.10 Hybrid precoding and combining architecture [60] 41
3.11 Analog part:(a) fully connected;(b) sub-connected with fixed sub-array;(c) sub-connected with dnamic sub-array [17]. 42
3.12 System model using 1-bit ADC precoding/combining [60] 43

4.1 Block diagram of the uth UT (transmitter) 47
4.2 Block diagram of the BS (receiver) 49
4.3 Performance of the proposed equalizer for 8 users and $s_M = 0.5$ 55
4.4 Performance of the proposed equalizer for 8 users and $s_M = 0.8$ 56
4.5 Performance of the proposed equalizer for 8 users and $s_M = 1.1$ 56
4.6 Performance of E_b/N_0 as function of the number of iterations 57
4.7 Required EbN0 to achieve target BER as function of s_M for each iteration 58
4.8 Performance comparison between 8 and 4 users for $s_M = 0.8$ 59
4.9 Performance of the proposed equalizer for 4 users and $s_M = 0.8$ 60
4.10 Performance of the proposed equalizer for 8 users and $s_M = 0.8$ 60
4.11 Performance of the proposed equalizer for 16 users and $s_M = 0.8$ 61

List of Tables

2.1 Linear equalizers characteristics 18

3.1 Attenuation of different materials [52] 35

4.1 Simulation parameters 54
4.2 Parameter values for simulated scenarios 55

Chapter 1

Introduction

This dissertation begins with an introduction to wireless communication systems, a brief historical insight is presented, culminating in the next generation of wireless systems (5G). In this chapter the key paradigms that are the backbone for the current and future development of wireless networks are presented. Second to that, the motivation and objectives of this dissertation are presented.

1.1 History

Telecommunications is a branch of technology concerned with the transmission of information over a distance, where the transmitter sends information to a receiver. For centuries, messages (information) were transported by messengers, who would carry them either by walking or transported by horse, or boat. Visual signs such as fire, smoke, sunlight mirroring and semaphores (such as the Chappe semaphore and the heliograph presented in figure 1.1) were used in rudimentary telecommunication systems.

Along with the dawn of electricity and the development of new electrical devices, telecommunications faced a never ending transformation. Thanks to the work developed by James C. Maxwell, particularly the Maxwell equations, presented around the year 1865 unifying the theories of Lorentz, Faraday, Ampere and Gauss. This set of differential equations describes the movement of electromagnetic waves in space and became a landmark in the development of radio technologies which endures to the present day.

In 1887, Heinrich Hertz invents the oscillator (AC generator) a device capable of generating radio waves, also providing understanding of the dipole antenna element. At the end of the nineteenth century, in 1895, the physicist and inventor Guglielmo Marconi used radio waves to transmit telegraph signals across the English Channel. Just 6 years later a similar transmission was made over the Atlantic ocean, digital radio communications were borne, with commercial transatlantic connections being deployed [3].

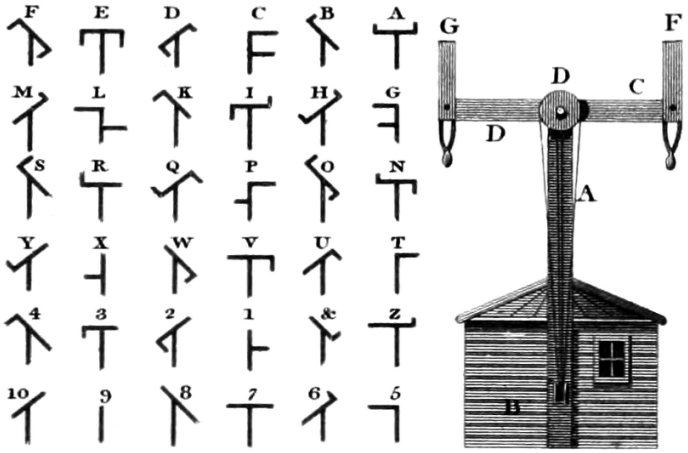

(a) Chappe semaphore and code of letters and symbols [1]

(b) Heliograph device [2]

Figure 1.1: Examples of pre-radio telecommunication systems

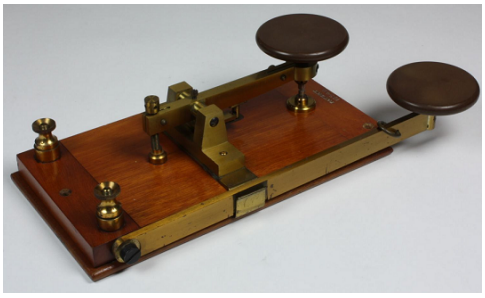

(a) Telegraph device [4]

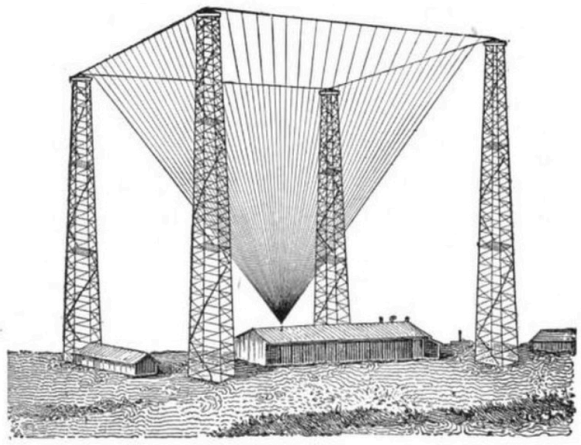

(b) Typical base station of the telegraph service [5]

Figure 1.2: The telegraph system

The beginning of the twentieth century also brought the first analog radio communications, used to transmit voice over radio channels(telephony). In the middle of the twentieth century, further development of transatlantic communications happened, with creation of the satellite based global communications system still used in present day. The concept of mobile communication also appeared within this timestamp, with the development, by Bell Labs, of the Mobile Telephone System (MTS) and the Ericsson's Mobile System A (MSA), primarily to be installed in automobiles or truck fleets due to the heavy weight of these systems [6].

The final quarter of the twentieth century witnessed a boom in wireless communications for personal use, mainly driven by the objective of adding mobility to the traditional telephone service and to add the portability component to local area networks. Different analogue cellular

Figure 1.3: Bell's MTS system, accommodated in the trunk of an automobile [6]

technologies emerged in Europe, USA and Japan, however, there was no compatibility between the systems and the user equipment had a considerable size and weight. These developments laid the foundation for the first generation of cellular communications (1G), this was an analog mobile phone system and the most prominent were the Nordic Mobile Telephony(NMT) in Europe, the Advanced Mobile Phone System(AMPS) in the US and the Total Access Communication System(TACS) in Japan.

In order to develop a European standard for digital cellular voice telecommunications, the Group Special Mobile committee - later renamed as Global System for Mobile communications(GSM) by the European Telecommunications Standards Institute(ETSI) - was created in the year 1983. The main benefits of GSM were the digital encryption, which brought safety improvements, the higher spectrum efficiency that allow for more users to establish connection and the compatibility with data services,introducing the Short Message Service(SMS) which allow for text messages to be transmitted. GSM system reached the market in 1991 and it has been used and upgraded to the present day, first by upgrading from circuit-switched transport to packet data transport via General Packet Radio Service(GPRS), and Enhanced Data Rates for GSM Evolution(EDGE) with significantly improved data rate allowing for new services such as Multimedia Messaging Service(MMS) and Wireless Application Protocol(WAP). GSM technology is still widely used, with nearly 2500 million devices connected to the GSM network worldwide in the year 2018 [7].

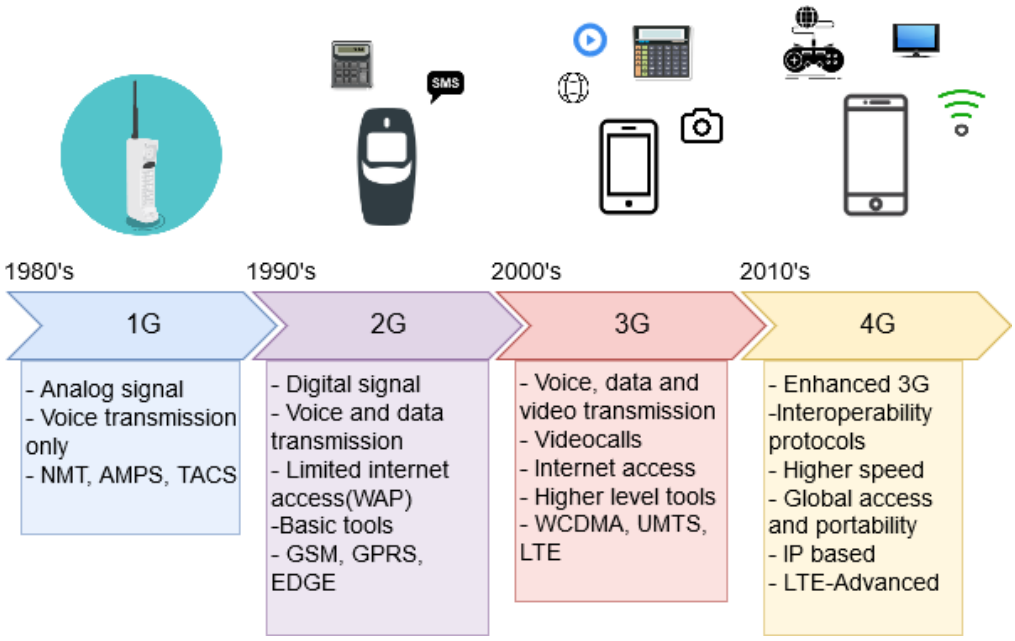

Figure 1.4: Evolution of wireless communications

The International Telecommunications Union(ITU) issued the requirements for the third generation of mobile communications(3G) to be part of the International Mobile Telephone 2000(IMT-2000) international project, for which new networks had to present significant improvements to the established 2G system such as mobile internet access videocalls and mobile TV. To cope with this task, the 3rd Generation Partnership Project(3GPP) was created, a joint standardization project between standardization bodies from Europe, Korea, Japan, USA and China to develop the Universal Terrestrial Radio Access(UTRA) system. This new technology employed WCDMA which supports two basic modes of operation, Frequency Division Duplex(FDD) and Time Division Duplex(TDD). In FDD, separated 5 MHz carrier frequencies are used for uplink(UL) and downlink(DL) respectively, in TDD one 5MHz carrier is time-shared between UL and DL. The primary 3G technologies were the Universal Mobile Telecommunications System-High Speed Data Packet (UMTS-HSPA) and CDMA2000. 3G brought a big technologic evolution in networking and data transmission with better connectivity and with increased spectrum efficiency capabilities of up to 2 Mbps [8] [9].

The paradigm for 4G was about convergence; convergence of of wired and wireless networks, wireless technologies including GSM, wireless LAN, and Bluetooth as well as computers and consumer electronics. 4G is a mobile multimedia, anytime, anywhere with global mobility support. 4G technologies were also required, as indication by ITU for the IMT-Advanced system, to be based on Internet Protocol(IP) for data traffic and minimum data rate of 100 Mbps. Soon after 4G, 4G - Long Term Evolution(4G-LTE) was introduced, which consisted on a redesign and simplification of the legacy 3G UMTS network architecture. 4G-LTE uses Orthogonal Frequency Division Multiple Access(OFDMA), which brings great benefits in terms

of spectrum efficiency, thus allowing for higher bandwidth, better performance and higher data rate. Current technologies associated with 4G are Evolved High Speed Packet Access (HSPA+) and LTE [8] [9].

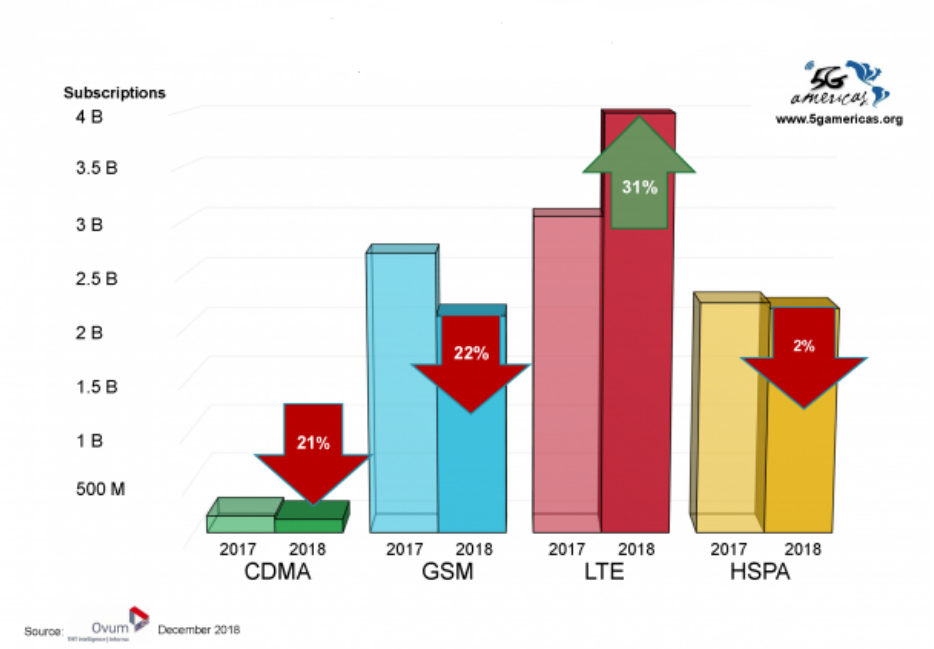

Figure 1.5: Annual global technology growth [10]

Figure 1.5 depicts the evolution in the number of connected devices, by technology, in the years 2017 to 2018. As 4G networks become widely available, LTE subscriptions have grown and will continue to do it in the next few years, until 5G systems are established. Much of this growth in LTE adoption is due to migration from older technologies, such as GSM and CDMA. A similar tendency is expected in the future. As 5G coverage becomes wider, more devices exploiting the new capabilities of this technology will be connected.

1.2 Future system 5G and beyond

The wireless world is increasingly demanding for effective management of the infrastructures in an energy-, spectrum- and cost-efficient manner. This has been the paradigm for wireless communications ever since the GSM committee was created, also adopted by the 3GPP. There are 7 technical directions that aim for achieving the requirements of current and future internet.

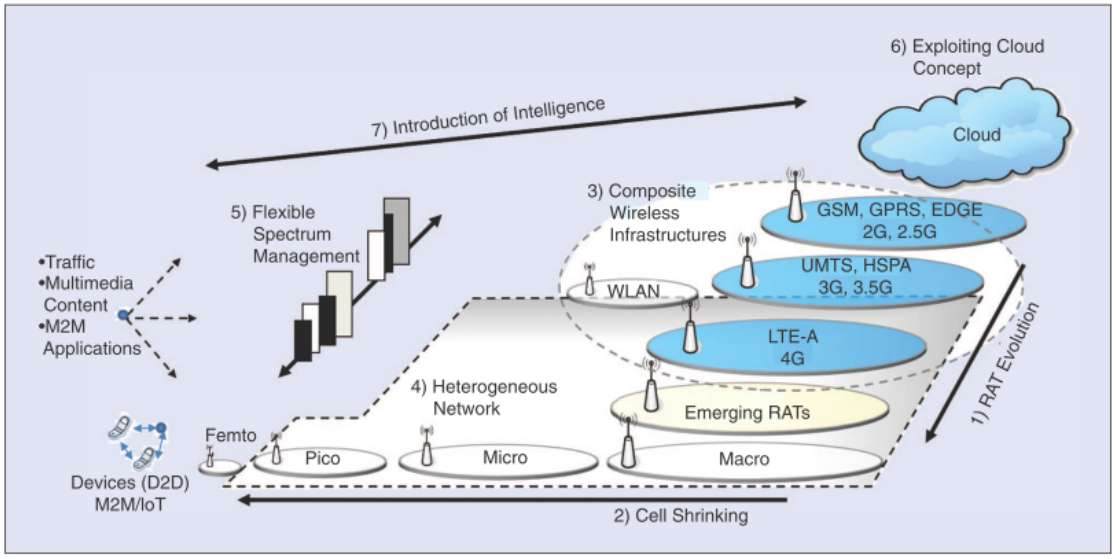

Figure 1.6: Technical directions of wireless evolution [11]

The first direction considered is the evolution of radio access technlogies (RATs), which led from a frequency/time division multiple access (FDMA/TDMA) and wideband code division multiple access(WCDMA) schemes, to orthogonal frequency division multiple access (OFDMA) schemes and to a more efficient use of radio resources (e.g. spectrum).

The second direction is the decreasing of cell size. This aims the improvement of the capacity and cost of the resources that are deployed as well as spectrum use. The cells vary from macro cells to more modern and smaller cells (pico-, femto-cells) as depicted in figure 1.7, that improve the capacity and have lower cost when compared to the older macro-cells.

A third direction, more recent, is the development of composite wireless infrastructures, which aims at the joint operation of heterogeneous wireless access infrastructure, as is example the interworking of cellular systems with WLANs as depicted in figure 1.7. The fourth direction is the deployment of heterogeneous networks, it is closely related to the previous one, however specialised in increasing the cost efficiency. This paradigm is focused on only one cellular standard such as 4G/Long Term Evolution(LTE)-advanced (even though IEEE standards may also apply under certain conditions). A heterogeneous network may consist of different types of infrastructure elements, such as macro-, micro, pico- or femto-cells or base stations (BSs). Heterogeneous networks offer multiple options for satisfying the application requirements and have a positive impact on the cost of the deployed resources and their utilization.

Another direction is the flexible spectrum management. Also targeted for the improvement of resource utilization, this paradigm consists in the allocation of spectrum in a flexible way in the various RATs. Key elements such as spectrum re-farming (setup communication on a specific RAT in different frequency bands, or the same frequency with sufficient spacing that there is no interference), opportunistic spectrum access (secondary users are allowed to independently

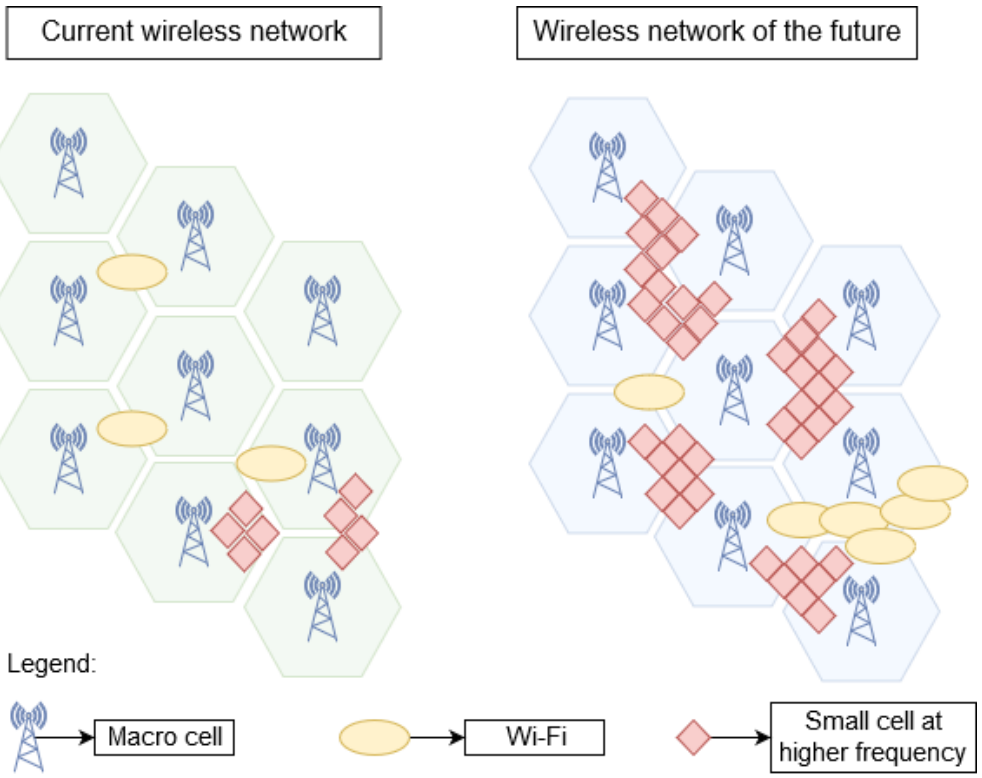

Figure 1.7: Heterogeneous networks, present and future

identify unused spectrum bands, at a given time and place, and use it without generating harmful interference to primary licence holders, e.g. TV white spaces). Other concepts, such as authorized-shared access (ASA) and licensed shared access (LSA) enable dynamic sharing of spectrum band in space and time; in addition, the collective use of spectrum (CUS) allows spectrum to be used by more than one user simultaneously without requiring a licence, examples of which are radio-frequency identification (RFID) and machine to machine (M2M) applications [12].

The sixth direction is the device-to-device (D2D) and machine-to-machine (M2M) communications, which is expected to characterize beyond 4G and 5G networks, aims for the creation of dynamic network structures consisting of interconnected end-user equipment or several machines/sensors/actuators in the context of the internet of things (IoT). Today, the number of connected devices is around 7 thousand million, roughly the same number of inhabitants on the planet, this number is expected to rise to around 97 thousand millions by the year 2030 [13]. Traffic generated from various M2M applications will have to be properly assigned to access points without causing congestion issues. Cognitive, intelligent management mechanisms will be necessary to efficiently control and maintain all these networked devices [11]. Figure 1.8 depicts the subscriptions forecast by technology for the upcoming years. Although LTE subscriptions are predicted to continue rising in the next few years, that tendency should invert as 5G technologies are deployed more widely. The total number of connected devices is expected to

steadily rise in the future, as depicted in figure 1.8, with an additional thousand million devices connected in the next five years, surpassing the total number of inhabitants on the planet. Much of the initial 5G subscriptions will be based on M2M and D2D communication. However, as more 5G networks are established, there will be a gradual increase in 5G connections to the detriment of older technologies.

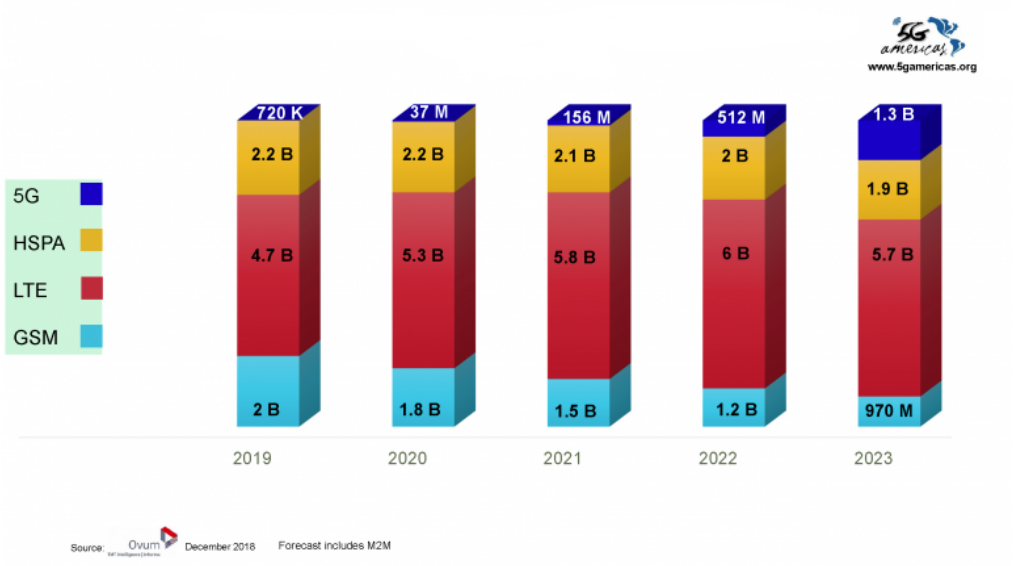

Figure 1.8: Annual global technology subscriptions forecast 2019-2023 [10]

At last, another direction is exploiting the cloud-radio area network(RAN) and mobile clouds, which aims to further improve cost efficiency, capitalized on cloud concepts. This paradigm sets on the rationale that there can be total cost of ownership savings if wireless networks are based on cloud principles, possible due to the shared use of storage and/or computing resources (e.g. Netflix). Common repositories for networking functionality can be used to avoid multiple deployment of the same component.

In order to achieve the previously mentioned directions/paradigms it is mandatory the introduction of intelligence in the heterogeneous network management. Intelligence is expected to facilitate decisions regarding: 1) transceivers that will be involved in the handling of a situation; 2) spectrum that will be assigned to be operated by the transceivers; 3) transmission powers that will be allowed per transceiver; and 4) distribution of traffic to the cell that are involved in the handling of the situation [11].In the future, advanced connectivity will provide new ways of innovating, collaborating and socializing. Already today, more than 60% of the world population has access to mobile communication and in the next few years more than 90% of the world's population will benefit from mobile broadband coverage.

Wireless communication systems have continuously evolved throughout the past decades, the interval between each significant technology platform has been about ten years. Within each platform, there is constant innovation, leading to continued improvement in speed, efficiency and

capabilities. Along with the deployment of the fifth generation of wireless/mobile broadband systems (5G), and 5G-New Radio(5G-NR) which comprises the new radio technologies that operate at higher frequencies, a multitude of devices will be interconnected and the traffic demand will constantly rise.

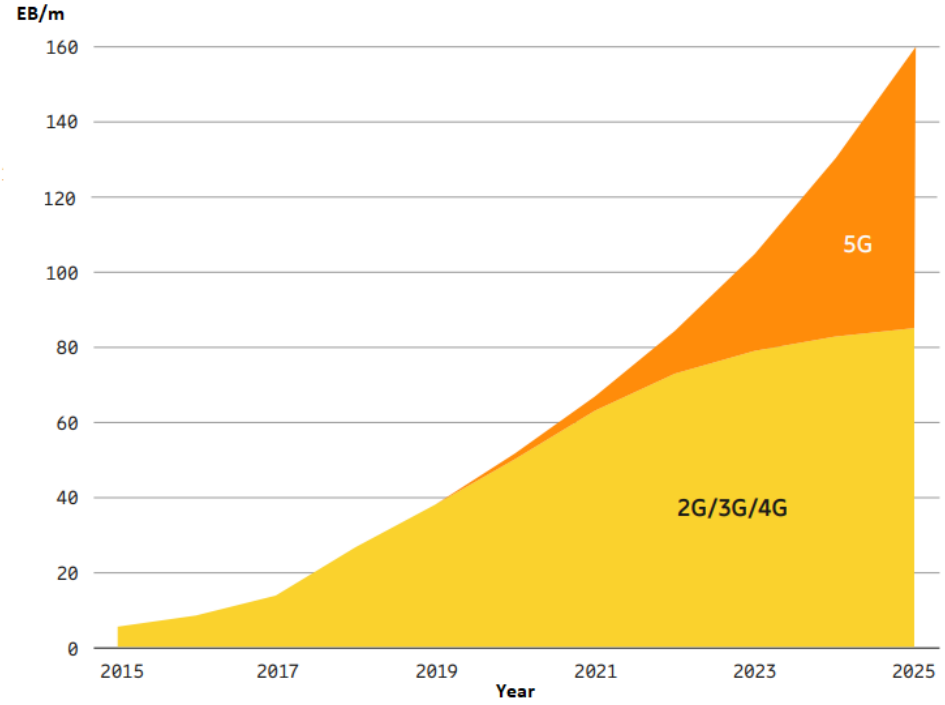

Figure 1.9: Global mobile data traffic in Exabytes per month [14]

Fueled by dramatic bandwidth expansion and data rate improvements, as well as increased connected devices, data traffic is expected to rise exponentially in the upcoming years. A four fold increase in data traffic, totalling 160 Exabytes per month until the year 2025 is predicted. Even though most of this traffic will be carried by 4G and previous technologies, 5G alone will take up to 45% of the global mobile data traffic within the next 5 years. Therefore, there are specific requirements that need to be fulfilled by the wireless network systems. The requirements issued by ITU for the IMT-2020 are auspicious. 5G systems should provide at least 10 times higher data rate compared to its predecessors, at least 100 Mbps regardless of location, and 1 Gbps for low mobility users; less than 5 milliseconds(ms) end-to-end latency; significant spectrum efficiency improvements; mobility of up to 500 Kilometers per second and 100 fold increase in capacity, just to enumerate a few. Other key requirements are shown in figure 1.10, which present a graphical comparison between 5G and 4G requirements [14].

Massive Multi-Input Multi-output (mMIMO) systems, equipped with hundreds of antennas, and operation at frequencies above 30 GHz are two key enabling technologies to achieve the QoS requirements of 5G. Operation at frequencies above 30 GHz, also called milimeter wave(mmWave) band due to its wavelength ($\lambda \leq$ 10milimeters), bring great opportunities.

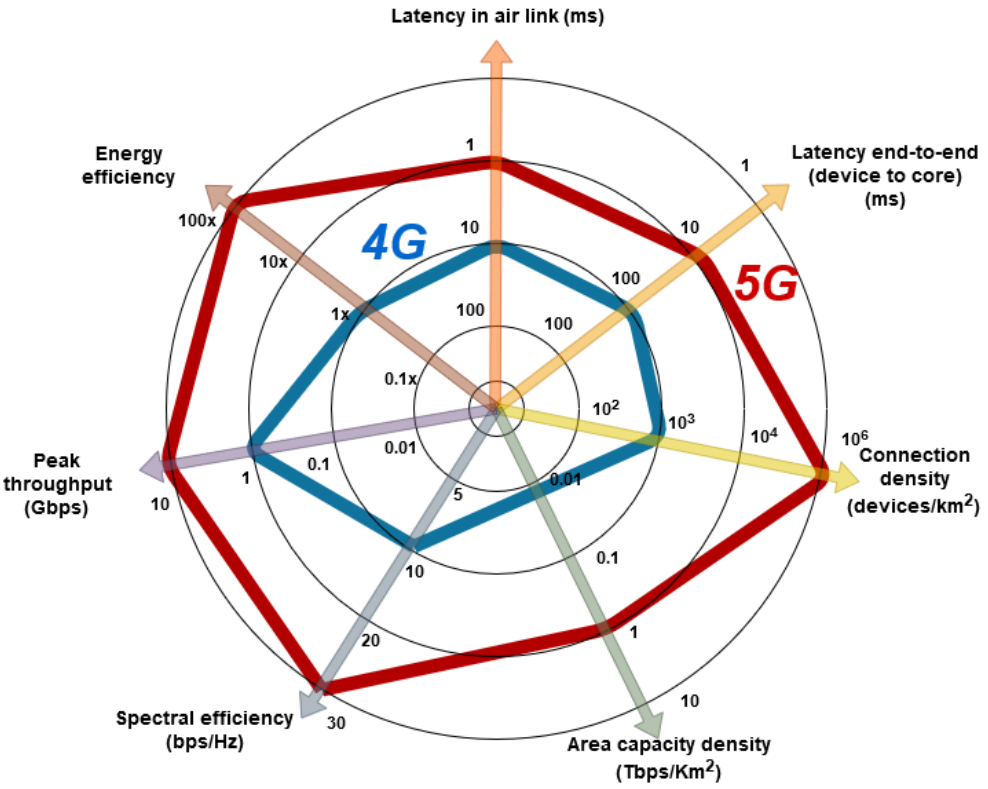

Figure 1.10: Performance requirements for 5G

Spectrum availability is scarce in current wireless communications, the vast majority of wireless communication or broadcast systems operate at carrier frequencies below 3 GHz, with few exceptions. Forecasting the exponential growth in cellular communications, operating in the mmWave band offers the possibility to exploit vast amounts of bandwidth that is available at higher frequencies. This can also derive in increased spectrum availability in sub-6 GHz band. The small wavelength of mmWave signals translates into smaller antenna size, this will allow for a very high number of antennas to be packed in small areas. This is the paradigm for mMIMO. Using a massive number of antennas allows for more degrees of freedom and transmission techniques can be refined, improving performance.

1.3 Motivation and objectives

The constant evolution of cellular systems has enabled an exponential growth in the number of connected devices around the world. Alongside this increase in connected users there is an increase in data traffic and QoS requirements. To cope with these requirements, milimeter wave (mmWave) and massive MIMO are regarded as key enabling technologies for the 5G and future internet systems. Operation in mmWave band is not a novelty, even though its use is currently confined for short range service and indoor communication.

The use of multiple antennas to increase the capacity and reliability of wireless systems is

already being employed, however, with the rise of interest in mmWave communications also brings new paradigms such as the use of a massive number of antennas in order to overcome the poor propagation characteristics of mmWave signals. In conventional MIMO systems, each antenna has a fully dedicated radio frequency(RF) chain since all processing is completed at the digital level. However, fully digital architectures are not feasible for a large number of antennas due to hardware limitations, and thus hybrid analog-digital architectures have emerged as options to keep a high number of antennas without as many RF chains. In the recent years, hybrid analog-digital beamforming for both sub 6-GHz and millimeter wave bands were proposed in [15–20] for which part of the signal processing is performed in the analog domain, and the reduced complexity processing is left to the digital domain.

Another aspect that must be taken into account is the energy needs of future wireless systems deployment, as the number of connected devices and data traffic rises exponentially it is mandatory that the transceivers consume the least required power possible and be the very efficient in terms of energy consumption. In order to be more energy efficient, the power amplifiers usually operate close to its saturation threshold, which causes it to behave in a non-linear fashion. This situation introduces distortion in the transmitted signals which in turn cause errors on the reception. Therefore it is crucial to evaluate these systems under non-linear distortion (NLD) caused by the amplification. Thus the main objective of this work is to design a hybrid iterative analog-digital equaliser which is able to cope with the NLD introduced due to operation in the saturation zone and the multi-user interference. The non-linear power amplifier response is assumed to follow an analytical model found in the literature [21]. The proposed iterative equalizer is designed by assuming the knowledge of the power amplifier characteristic that is used to remove distortion. The results show that the proposed scheme is able to effectively reduce the effects of NLD and multi-user interference with a few iterations and thus improving the performance of the system.

1.4 Document structure

The remainder of this dissertation is organized as follows:

Chapter 2 presents a brief introduction of the modulation schemes employed in current systems which would be the base of 5G, as well as the main multiple antenna techniques and the advantages that these bring. Power amplifier devices are also discussed in this chapter, analytical models that approach power amplifier characteristics are presented, and the NLD that derive from its operation is also introduced. At last, an insight regarding interference cancelation and the concept of IB-DFE is presented.

Chapter 3 presents insights in mmWave systems and massive MIMO deployments. It is discussed the particular characteristics that operation at mmWave brings to the signal propagation.

Use cases for mmWave communications are also presented. The benefits and main challenges of mMIMO technology are also discussed in this chapter. Hybrid analog-digital techniques for signal precoding and combining in mmWave are presented as well as energy efficient solutions - such as the use of low resolution analog-to-digital converters (ADC) and digital-to-analog converters (DAC) - that can be incorporated in future wireless systems. This chapter, joined with the second chapter aims to present essential background for the subject addressed in the development of this dissertation.

In chapter 4, a detailed description of the implemented massive MIMO mmWave system is given. The iterative hybrid analog-digital equalizer is derived an thoroughly discussed. The results are presented in terms of bit error rate (BER) to evaluate the performance of the proposed equalizer and algorithm. It is demonstrated that the proposed system is able to mitigate the NLD and multi-user interference effects in just a few iterations.

At last, in chapter 5, the conclusions of this work are presented. Some guidelines for future research are also suggested.

1.5 Notations

The used notation for mathematical expressions is given as follows, capital boldface letters denote matrices and lower boldface letters denote column vectors. The operations $tr(.)$, $(.)^*$, $(.)^T$ and $(.)^H$ represent the trace, the conjugate, the transpose and the Hermitian transpose of a matrix, respectively. The functions diag($\mathbf{a}$) and diag($\mathbf{A}$), where $\mathbf{a}$ is a vector and $\mathbf{A}$ is a square matrix, correspond to a diagonal matrix where the entries of the diagonal are equal to $\mathbf{a}$, and to a vector equal to the diagonal entries of $\mathbf{A}$, respectively. The element of the nth row and mth column of $\mathbf{A}$ is denoted $\mathbf{A}_{(n,m)}$ and the $N \times N$ identity matrix is denoted has $\mathbf{I}_N$; t, k and u represent the time, sub-carrier and user indexes, respectively.

Chapter 2

State of the art

This chapter presents an insight on topics relevant to the subject of this document. Firstly, the modulation schemes used in current cellular communications are presented. In the second section of this chapter, multiple antenna systems are revised, with additional focus in multi-input multi-output arrangements. Sections 3 and 4 are focused in power amplification and the impact that an energy efficient operation brings to the performance of radio frequency (RF) wireless communication systems. Behaviour models of the power amplifiers (PA) are presented, as well as techniques employed to reduce the distortion that derives from the amplification. Lastly, in section 5, a brief introduction regarding interference cancellation, and the concept of iterative block-decision feedback equalization(IB-DFE) which is used in the development of this project are presented.

2.1 Modulation schemes

Due to the increased demand for higher data rates and network availability in the first years of the past decade it was mandatory to develop better systems for wireless communication, which would overcome the limitations of traditional low throughput, low efficiency single carrier systems (e.g. FDMA).

To transmit data over a single carrier system, the signal can be modulated in phase, amplitude or frequency (depicted in figure 2.1) by a given carrier. In this way, to achieve high data rates implies a high symbol rate and thus high bandwidth and due to the tendency of mobile radio channels to be dispersive and time-variant poses great limitations to single carrier systems. In order to overcome these limitations, multicarrier systems have been developed to cope with the requirements of the UMTS and LTE systems.

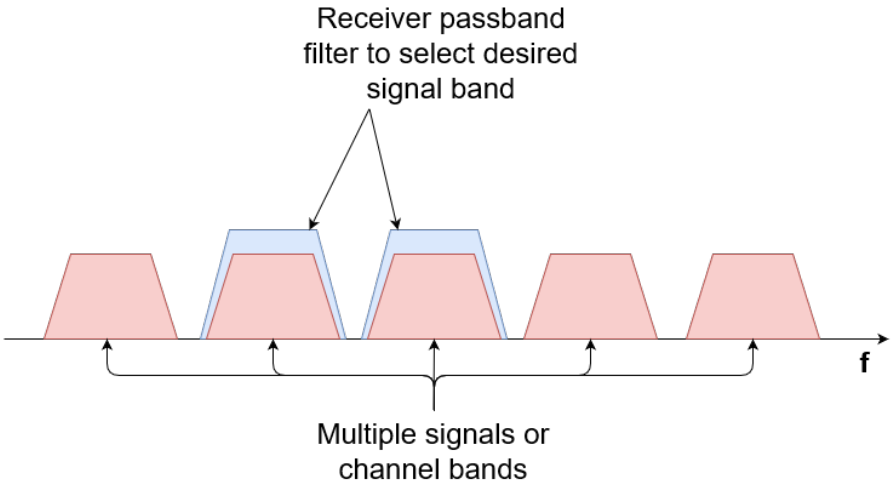

Figure 2.1: Basic principle of FDMA

2.1.1 Orthogonal frequency division multiplexing

Orthogonal frequency division multiplexing (OFDM) is the motor driving cellular communications nowadays, its high resistance to multipath effects and simplicity made OFDM the chosen modulation scheme for the 3GPP-LTE standards for 4G. Using low complexity digital signal processing, it is possible to modulate multiple subcarriers in an orthogonal fashion, meaning that there is some overlapping between contiguous subcarriers, however, when a given carrier central lobe is at its peak, the sidebands of the other carriers are at their minimum (figure2.2), thus eliminating inter-carrier interference (ICI) while increasing bandwidth efficiency since there is no need for a guard band [22].

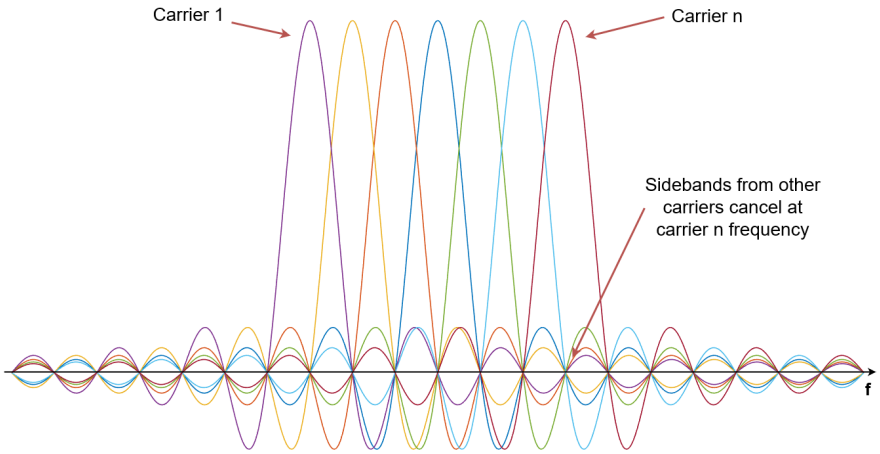

Figure 2.2: Multicarrier arrangement in OFDM

OFDM architecture

In OFDM, most of the processing can be done in parallel in the frequency domain, by applying the discrete Fourier transform(DFT) operation to each of the N_c carriers, which reduces significantly the complexity of the transceivers, therefore deployment cost. In figure 2.3 is depicted the block diagram of a typical transceiver for OFDM.

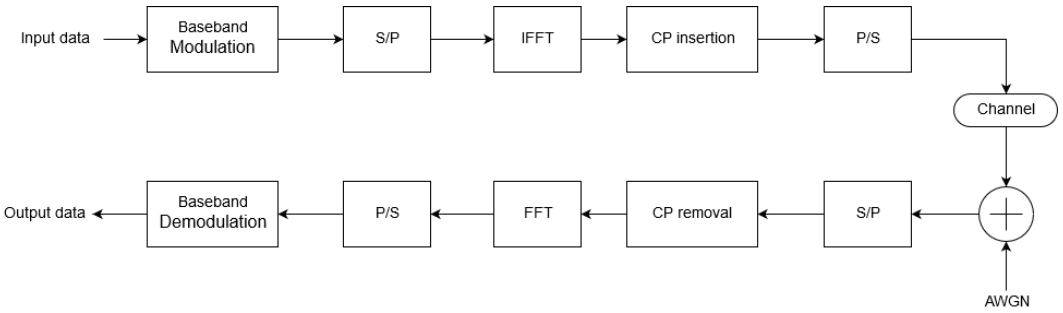

Figure 2.3: Transceiver structure of a typical OFDM system

Even though the orthogonality between carriers in OFDM systems solves the ICI problem, there is still inter-symbol interference (ISI) due to multipath delay of the signal. In order to solve this problem, it is necessary to add a guard band, thus the cyclic-prefix (CP) method was developed. It consists of adding a small copy of the end of the transmitted symbol to its beginning as depicted in figure 2.4.

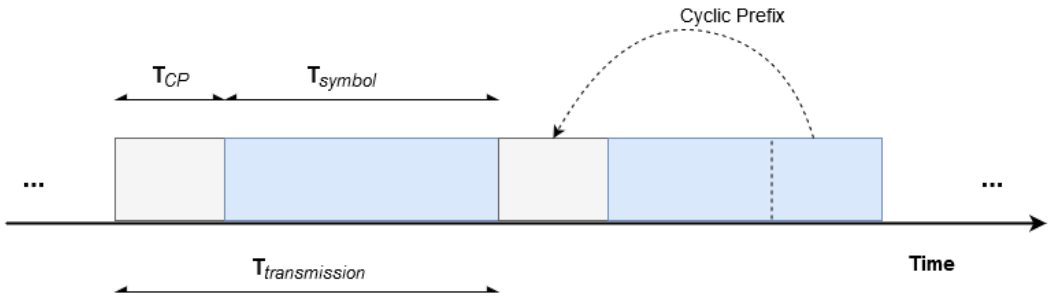

Figure 2.4: Cyclic-prefix method to overcome ISI

If the CP duration is higher than the maximum path delay, ISI is effectively avoided. It is clear that this ISI elimination comes with loss of symbol rate, because adding the CP rises the duration of each symbol transmission which is further exaggerated as the path delay increases. The CP is made of a portion of the transmitted symbols in order to maintain circularity, which in turn allow for low complexity frequency domain equalization.

In [23] a simple technique is used, in which by adjusting the sample rate of the OFDM symbol it is possible to increase the length of the CP (usefull OFDM symbol is shortened) and therefore accommodate the multipath delay, thus avoiding ISI.

OFDMA

Orthogonal frequency division multiple access (OFDMA) is a technique, based on OFDM, which provides multiplexing operation of user data. The main advance in OFDMA related to OFDM is that, in OFDM systems, there is user separation in time only, meaning that the full bandwidth is allocated to a single user in a given instant and in OFDMA users are separated both in time and in frequency, as depicted in figure 2.5, allowing for a more efficient allocation of resources, e.g., transmit only in specific bandwidth were a given user has a better radio link as other users.

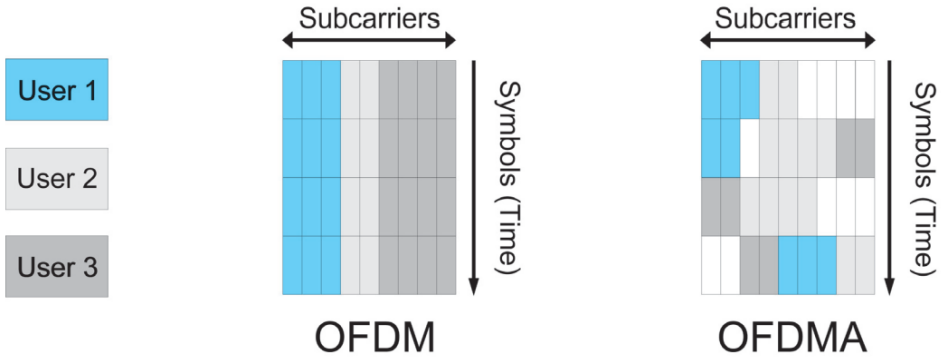

Figure 2.5: OFDM and OFDMA allocation schemes [24]

OFDMA offers key advantages in its implementation relative to other multiple access schemes (TDMA, CDMA), which made OFDMA the chosen scheme for current cellular deployments, namely [25]:

- Scalability - adjustable FFT size to channel bandwidth while fixing the subcarrier spacing and symbol duration minimizes impact in higher layers when scaling bandwidth;
- Robustness to multipath - similarly to OFDM, as long as multipath delays are within the CP window;
- Downlink multiplexing - improvements in downlink capacity due to efficient allocation of ressources (e.g., spectrum);
- Uplink multiple access - access performed through orthogonal sub-channels while taking advantage of frequency selectivity by allocating best sub-channels to respective access users;
- MIMO benefits - processing of OFDMA signals provide frequency flat channels, thus, full MIMO technologies can be easily deployed in conjunction with OFDMA.

To achieve the above mentioned advantages, OFDMA relies on precise frequency synchronization, because subcarrier spacing is typically small it makes OFDMA more sensitive to frequency

offset and phase noise, especially at high mobile speed due to Doppler effect [26].

2.1.2 SC-FDMA system

Due to the high PAPR that characterizes OFDM systems, it is not the most effective scheme to be used for the uplink transmission, the user terminals (UTs) are mostly cellphones, which have a limited battery so it is important that these devices have a more energy efficient manner to transmit data. The chosen scheme for the uplink transmissions according to 3GPP standard was SC-FDMA, which maitains the robustness to multipath fading of the OFDM systems with the low PAPR that characterizes the single carrier systems [27].

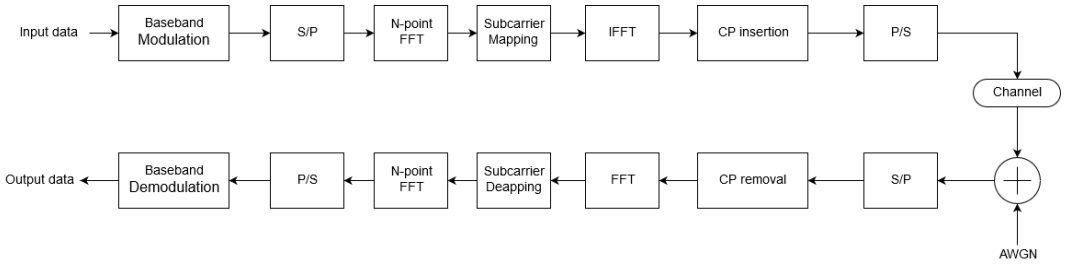

Figure 2.6: Transceiver structure of a typical SC-FDMA system

SC-FDMA, in the other hand, requires equalization of the received signal in order to properly reconstruct the data. There are a few different methods for equalization of the received signal such as:

- Maximal ratio combining(MRC);
- Equal gain combining(EGC);
- Zero forcing equalizer(ZF);
- Minimum mean square error equalizer(MMSE);

MRC and EGC offer the most simple implementation, however, their performance is not good as the equalizers fail to restore the orthogonality of the received signal. The ZF method is capable of restoring orthogonality and it is a low complexity solution, but if the channel is not well conditioned the noise enhancement rises causing estimation errors [28] [29].

Table 2.1: Linear equalizers characteristics

Equalizer	Model	Advantages	Limitations
MRC	$G_k = H_k^*$	Trivial implementation;	Orthogonality not restored, bad performance;
EGC	$G_k = \frac{H_k^*}{\lvert H_k^* \rvert}$	Trivial implementation;	Orthogonality not restored, bad performance;
ZF	$G_k = \frac{H_k^*}{\lvert H_k^* \rvert^2}$	Simplicity	Noise enhancement in the presence of nulls in frequency response of the channel;
MMSE	$G_k = \frac{H_k^*}{\lvert H_k^* \rvert^2 + \frac{1}{SNR}}$	Trade-off between noise enhancement and interference, better overall performance.	More complex, increased signal processing;

A more complex and effective approach is the MMSE method, which aims to minimize the square error, therefore overcoming the problem of deep fading channel response. For small values of SNR the noise is not enhanced and when SNR is high this method tends to the ZF method [30]. Table 2.1 presents the characterization of the above mentioned equalization methods where H_k is the frequency response of the channel at kth subcarrier and the operator (*) represents the conjugate.

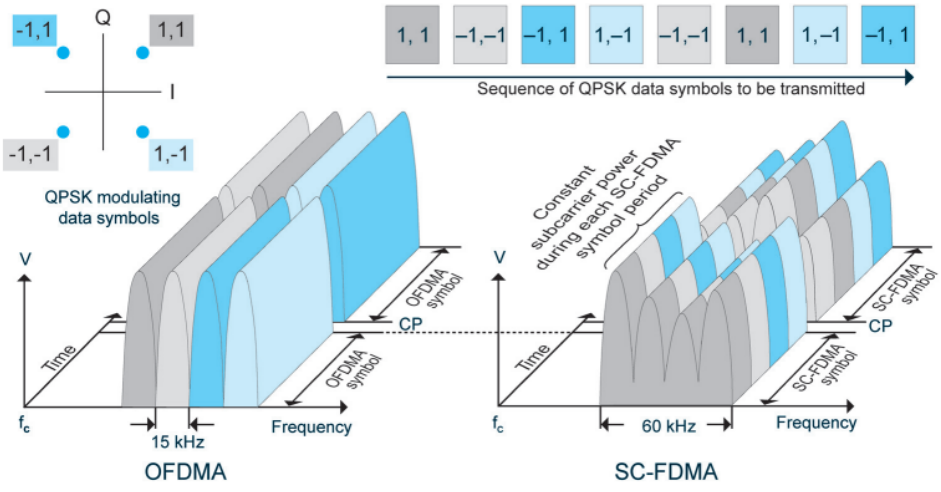

Figure 2.7: Transmission methods of OFDM and SC-FDMA - comparison [24]

As can be observed in figure2.7, in OFDM the multiple subcarriers are closely spaced together, with each symbol being assigned to each subcarrier to be transmitted over a period of time. In SC-FDMA case, the ocupied bandwidth is Ns times bigger, however, each symbol

requires only $1/Ns$ transmission time. In this way, OFDM and SC-FDMA achieve a similar throughput.

2.2 Multiple antenna systems

The concept of multi-input multi-output (MIMO) for wireless communications consists in the use of multiple antennas or antenna array aiming to increase the throughput of the system[12] or to improve reliability [31]. In the case of single-input single-output (SISO) systems, the channel capacity is given by the Shannon's channel capacity formula [32]:

$$C = f_b \times log_2(1 + \frac{S}{N}) \tag{2.1}$$

This equation implies that the system throughput, despite linearly increase with the bandwidth f_b, it increases logarithmically with the signal-to-noise ratio (SNR). This imposes great limitations for the SISO systems, since bandwidth efficiency can only be improved at the cost of power efficiency and *vice versa* [32].

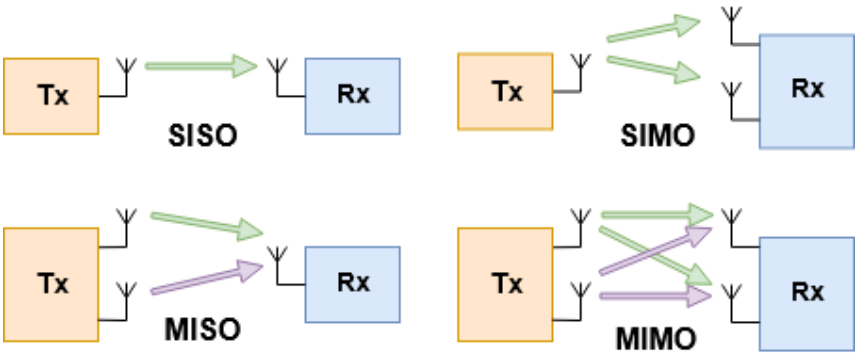

Figure 2.8: Single or multiple antenna arrangements

MIMO technology was an important advance for 4G cellular systems and is a key technology for 5G systems, jointly with mmWave. MIMO systems employ multiple antennas on the transmitter and receiver side, as depicted in figure 2.9, where N_{tx} and N_{rx} represent the number of transmitter and receiver antennas, respectively. The received signal can be obtained through the following expression:

$$\mathbf{y} = \mathbf{H}\mathbf{x} + \mathbf{n}, \tag{2.2}$$

where the transmitted signal $\mathbf{x} \in \mathbb{C}^{N_{tx}}$, the channel $\mathbf{H} \in \mathbb{C}^{N_{tx} \times N_{rx}}$, and the noise $\mathbf{n} \in \mathbb{C}^{N_{rx}}$ are used to obtain the received signal $\mathbf{y} \in \mathbb{C}^{N_{rx}}$.

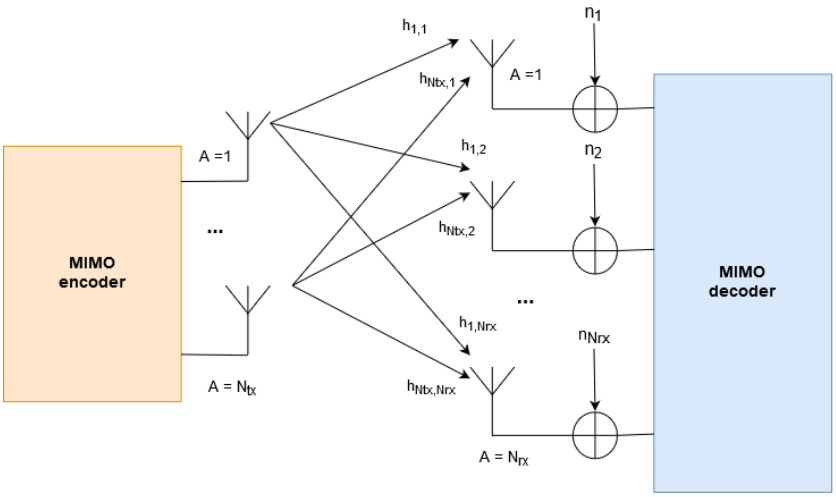

Figure 2.9: Generic representation of MIMO system

With MIMO sistems, capacity has shown to be proportional to the minimum of the number of antennas on each terminal (UT or BS) without requiring extra bandwidth or transmission power.

2.2.1 MIMO techniques

MIMO techniques can be classified into four categories, depending on the desired function of the system:

- diversity - same signal is sent/received over two independent channels, if one channel faces deep fading it is likely that others do not. Diversity can be achieved in space, time and frequency;
- multiplexing - different signal sent simultaneously over different antennas;
- beamforming - group of antennas generating a signal beam through constructive/destructive interference ultimately eliminating inter-user interference [33];
- multiple access - receiver antennas assigned to multiple transmitters, UTs, sharing the access medium;

In figure 2.10 a graphical description of the above mentioned MIMO techniques is presented. When there are multiple antennas on the receiver (receive diversity) or/and on the transmitter (transmit diversity), diversity gains can be achieved. Diversity gains can be achieved either in time, frequency, space or polarization. The idea is to send the signal over independent fading paths, which will most likely experience distinct fading, and combine all paths on the receiver to mitigate fading effects. Time diversity consists of sending the same information at different timestamps if those are separated by more than the coherence time. This code is redundant,

thus resulting in a loss of data rate proportional to the number of symbol repetitions. Frequency gains consist in transmitting the same narrowband signal in different carriers, where the carriers are separated by more than the coherence bandwidth. The main drawback of this technique is that it requires more bandwidth. In order to achieve space diversity, the antennas are required to be distant enough that the arriving signals experience distinct fading effects.

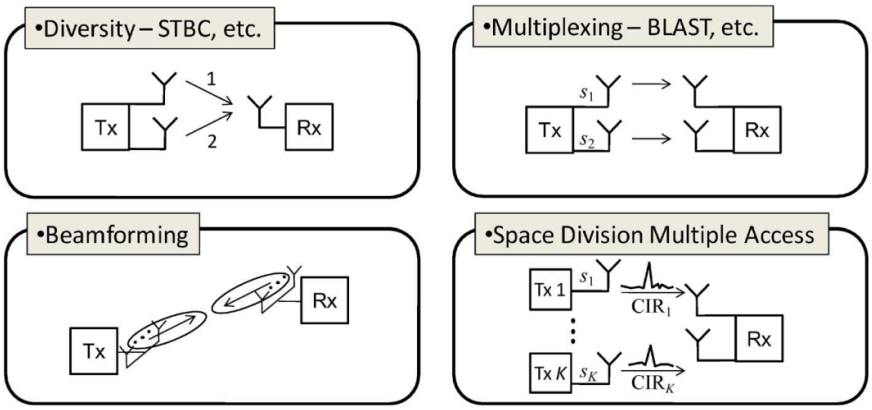

Figure 2.10: MIMO techniques [32]

In order to achieve receive diversity, equalization techniques such as selection combining(SC), equal gain combining(EGC), among others, can be applied in order to combine the signals received by the receiver antennas. Receive diversity can achieve space diversity or antenna gain, depending on separation of the antennas. Receive techniques are most common for the uplink transmission, since it is easier to have multiple antennas on a base station(BS) than in a user terminal(UT), as well as the required processing capabilities.

There are two ways to achieve transmit diversity, closed-loop transmit diversity and open-loop transmit diversity. In the first case, two or more copies of the signal are sent applying phase shift to one or more signals before transmission, thus reducing the risk of destructive interference. The channel state information (CSI) is available at the transmitter and the receiver assists in channel estimation and communicates these estimates to the transmitter.

When there is no CSI availability on the transmitter, open-loop transmit diversity is required. This can also be applied to adverse channel conditions, the performance is usually lower compared to closed-loop, however, it is a more robust approach. Equalization techniques based on encoding blocks of data, such as space-time/frequency block coding (STBC or SFBC) and space-time Trellis codes (STTC) are used. In these techniques, the transmitted data symbols are arranged in a way that they are orthogonal to each other. STTC performs better tha STBC ot SFBC, however, its high complexity limits the implementation in practical systems. A well known STBC technique, the Alamouti scheme, is demonstrated in [34]. The limitation of these orthogonal codes, is that they can only be applied for two transmit antennas. When the system

has more than 2 transmit antennas, Tarokh orthogonal code or Quasi-orthogonal codes are used. These techniques usually require bandwidth expansion.

MIMO multiplexing techniques are used to increase massively the throughput of a system, nevertheless, an excess of receive antennas can be used to reduce co-channel interference. If the antennas are separated by more than $\lambda/2$, spatial gains can be achieved by dividing and transmitting consecutive data symbols over all N_{tx} antennas. One well know example of MIMO multiplexing technique is the Bell Lab's space-time (BLAST) scheme, aiming for maximize the throughput of a single user [35]. Spatial division multiple access (SDMA), although related to previously mentioned multiplexing schemes, aim for the maximization of the number of supported users. This scheme shares the throughput of the system among all supported users [32].

Beamforming (BF) is a key enabling technology for the future of mmWave wireless communications. In order to overcome the increment in path losses characteristic to mmWave and transmit mmWave signals efficiently, the energy radiated by the antennas is (mostly) concentrated on a single beam. The conjugation of BF and mMIMO systems bring great opportunities for future wireless communications, which will be subject of more detailed discussion in chapter 3.

2.3 Power amplifier

The power amplifier (PA) is a key component for transmitting data using radio technology. Its function is to feed the antennas with the necessary energy for the transmission, by adjusting the power fed to an antenna during transmission in order to overcome path loss. PAs can be classified according to the time period on which the amplifier is effectively conducting power, this period is also referred to as conduction angle, being 360° (2π) a conduction angle corresponding to full period conduction, which is the characteristic of a class A power amplifier. Other classes of amplifiers as well as their conduction angles and maximum efficiency are depicted in figure 2.11 [36].

The most commonly used classes of linear PAs are A, AB, B and C, that also correspond to linear amplifiers, other types of amplifiers exist. Class D to T amplifiers are non-linear switching amplifiers with specific applications.

The PA is also the most energy consuming component of the system. Therefore, in order to obtain maximum power efficiency, the PA is operated near saturation point. Operation in this region introduces unwanted distortion to the in-band signal as well as unwanted additional frequencies in adjacent bands, which is further exaggerated due to high peak-to-average power ratio (PAPR) of the input signal.

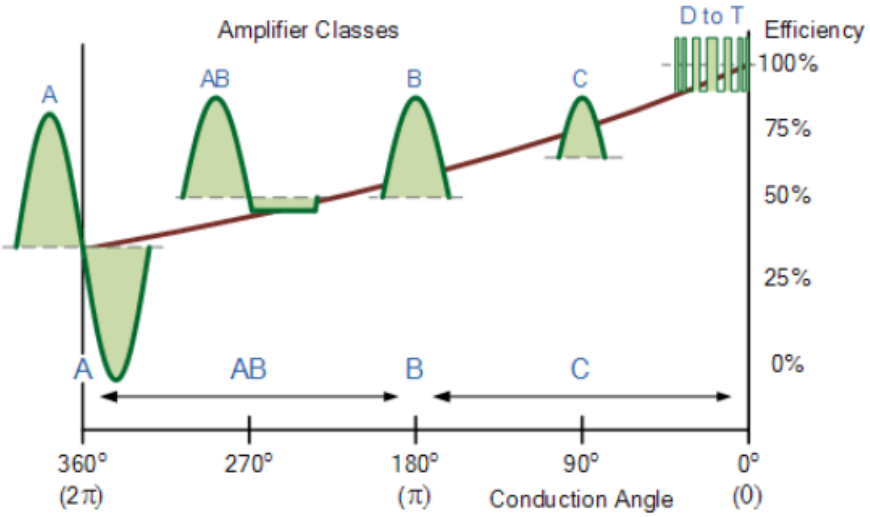

Figure 2.11: Amplifiers classes and efficiency [36]

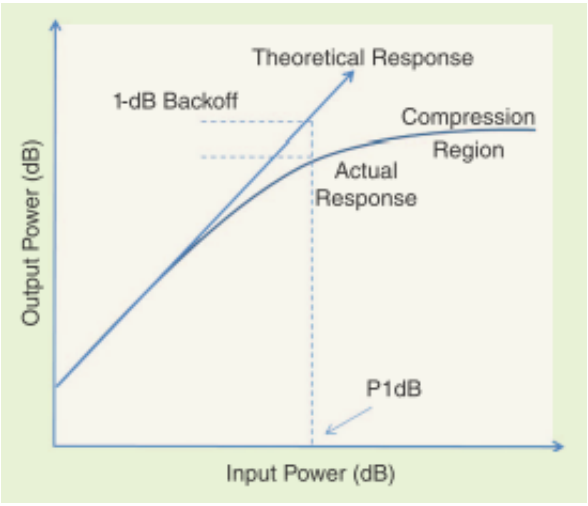

Figure 2.12: Linear PA behavior with saturation [37]

A PA is characterized by certain parameters or metrics which define its performance. Some are related to standard design requirements, such as power gain and frequency response but there are other key parameters used to design a PA [37].

Examples of such parameters are:

- Output power - the maximum power delivered to a load, within the interested frequency band;
- PAPR - the ratio between the peak output power and the average output power within the interested frequency band;
- P1dB point - 1 dB compression point, the input power at which the amplifier's gain falls 1 dB bellow its linear gain specification, see figure 2.12, and it is considered to enter its

saturation region;

- Adjacent-channel power ratio - when amplifying the main channel signal, some power also leaks to adjacent channels. Adjacent-channel power ratio (ACPR) is the ratio between the power leaked to adjacent channels and the root-mean-squared (rms) power of the main channel signal.

A given PA can be modelled mathematically by defining the above mentioned parameters in order to understand its behaviour in the saturation zone. This approach considers the PA as a "black box" relying exclusively on carefully chosen input-output observations to model the PA non-linearities [38]. Applying this method, a theoretical behavioural model for the PA is created, taking in account that the PA can be modelled as a memoryless system, which is usually the case in OFDM systems [37]. There are several PA behavioral models, of which, three are regarded as the most commonly used:

- Saleh model - simple static PA model, used with high power amplifiers, such as the traveling-wave tube amplifier (TWTA);

- Solid-state PA model (SSPA) - model used for medium/low-power amplifiers, similar to limiter model if 'p' (smoothness of transition) is high;

- Limiter model - used to cut off the signal above a certain threshold value.

The choice of any of the above methods must take in consideration the output power, packaging and applied power. Microwave telecommunications industry primarily relied heavily on TWTA and this model provides reliable performance and greater lifetime than SSPA, being still used in radar, broadcasting and communications. SSPA models have shown to be more suited to model low and medium PAs [39], which are predicted be used in most of future massive MIMO wireless deployments, thus the ones studied in this work. One such example of a SSPA model and widely used is the Rapp's model. Two of the most important estimators of the power amplification impact on communication systems linearity performance are the amplitude modulation/amplitude modulation(AM/AM) and the amplitude modulation/phase modulation(AM/PM) conversion functions [40]. The non-linear amplifier response transforms the time signal $x_n^{'}$ into the signal $z_n^{'}$, where $x_n^{'}$ is the time-domain signal equivalent of the OFDM signal, i.e. $x_k^{'}$, as depicted in figure 2.13. The PA output can be given as function of the AM/AM and AM/PM functions, using equation 2.3.

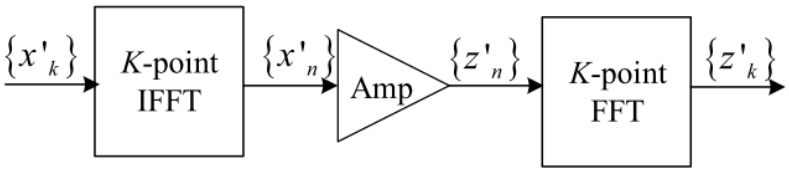

Figure 2.13: Block diagram of non-linear amplification

$$z_n = f_A(|x_n|)e^{jarg(x_n)+jf_P(|x_n|)} \tag{2.3}$$

where f_A and f_P are the AM/AM and AM/PM non-linear conversion functions, respectively. This signal thus includes the non-linear effect of the PA. In Rapp's model, f_P is approximately zero and f_A is given by the expression [41]:

$$f_A(r) = \frac{r}{\sqrt[2p]{\left(1 + \left(\frac{r}{s_M}\right)^{2p}\right)}}, \tag{2.4}$$

where p is the parameter that controls the smoothness of transition between the linear and saturation regions, r is the absolute value of the PA input signal and s_M is the output value in the saturation amplitude.

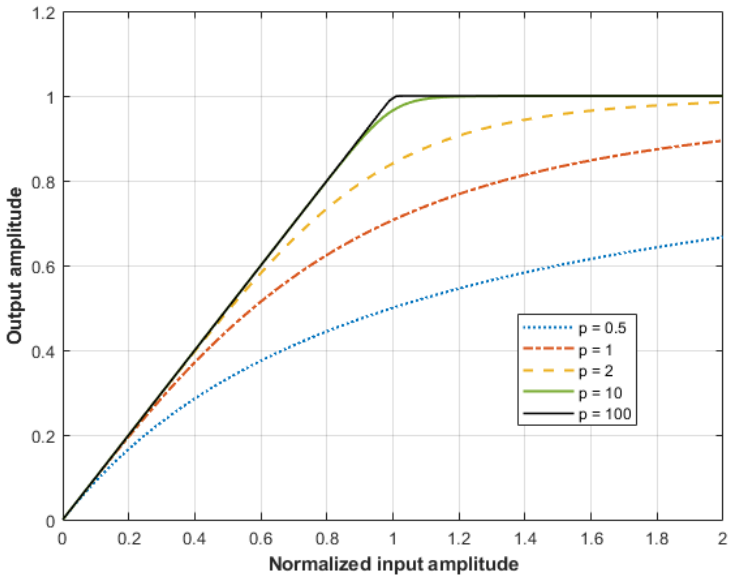

Figure 2.14: Output amplitude vs Input amplitude for Rapp model of PA [42]

Figure 2.14 depicts the relation between input and output amplitude of the Rapp model of a PA as well as the influence of p in the smoothness of the transition. A realistic value for this parameter is $p = 3$.

2.4 Non-linear distortion

In order to make wireless transmission equipments more energy efficient, the PAs of the systems usually operate close to the saturation zone, causing the PA to behave in a non-linear way, provoking NLD which in turn causes in-band and out-of-band distortion thus degrading the BER performance and interfering with adjacent frequency bands.

The NLD has a significant negative impact in telecommunications systems performance. Several techniques are used in order to mitigate the effects of the NLD, also know as linearisation techniques such as backoff linearization, PA non-linearity cancellation (PANC), clipping and filtering. Other aspects that impact the wireless channel, thus increasing the negative impact of the NDL are the high PAPR that characterizes OFDM based systems, and fading [21]. In order to improve the throughput, some linearization or non-linearity cancelation techniques are necessary. Although many solutions are available, the most commonly used techniques for NDL mitigation include [37]:

- Backoff linearization - simple implementation. Increases power backoff, resulting in the PA working in a more linear region, thus, reducing power efficiency. Less applicability in modern/future systems.
- Clipping and filtering - limits the signal under a certain threshold, and filters out the out-of-band distortion that results from it, reducing spectral spreading. It is the optimal solution when a linear PA is used.
- Feed-forward linearization - minimizes the non-linear effects of the PA, keeping it within its linear region.
- PA non-linearity cancelation (PANC) - a model of the PA is created and NLD is quantified and canceled, used together with combining/equalization techniques in cooperative systems can sigificatively improve the performance of an OFDM system.

2.5 Interference cancelation

Hardware components of a RF front-end are prone to wearing down, causing those to behave in unexpected ways, which, in addition to the inherent imperfection of real systems, lead to a great performance penalty of RF systems due to non-linearities [43].

An effective way to improve performance of a RF system is to force the PA to behave in a more linear way. This can be achieved by means of pre-distortion. In the case of transmitter NLD cancelation, a given model of the PA is computed (e.g. Rapp model) and a pre-distortion block with inverse characteristics is applied to the signal before it is amplified, resulting in the PA to behave as depicted in figure 2.15.

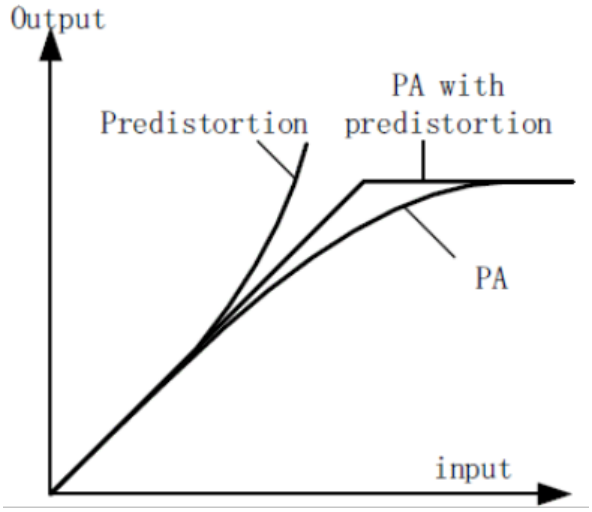

Figure 2.15: Linear PA behavior with applied predistortion [43]

In [44] and [45] two distinct interference cancellation technique are used on the receiver side, where given an initial estimate of the transmitted symbols, the distortion effects can be estimated if he PA model is know, after that, NLD can be removed from the received signal and new and improved symbol estimates can be obtained. This procedure can be repeated in an iterative manner to obtain symbol estimates with residual distortion with a reduced number of iterations. Another well know technique for interference cancelation on the receiver side is the iterative block-decision feedback equalizer (IB-DFE) which is presented below.

2.5.1 Concept of IB-DFE

IB-DFE schemes are the most successful non-linear frequency domain equalization techniques and have been widely used in the past decade in a variety of scenarios, namelly SC-FDMA systems used for the uplink communications of the LTE cellular system [46]. IB-DFE can be regarded as low complexity turbo equalizer implemented in the frequency domain and does not require the channel decoder output in the feedback loop.

In [46], two iterative approaches of the IB-DFE concept are studied: Successive Interference Cancellation (SIC) and Parallel Interference Cancelation (PIC). The first approach consists in the detection of all the K users on the lth subcarrier in a successive way, using the most recent estimation of the transmitted data symbols associated to each UT in order to cancel the corresponding interference. A block model of this approach is depicted in 2.16. The main drawback of this SIC approach is the larger delay in the detection procedure when compared to the PIC scheme, due to the sequential detection of the UTs. This is a major issue when implementing a practical system.

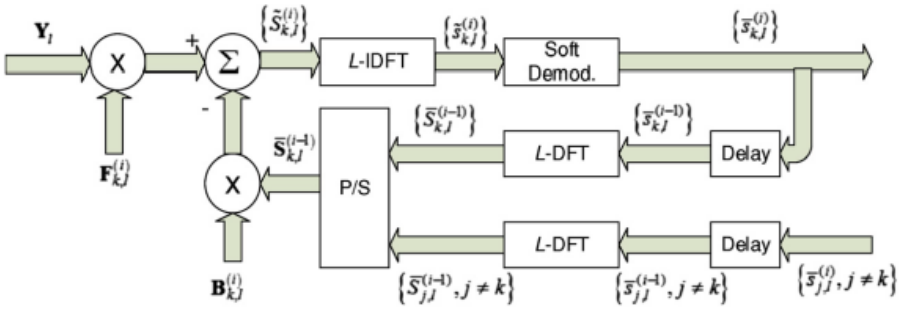

Figure 2.16: Iterative receiver structure based on IB-DFE SIC approach [46]

As for the PIC based approach the detection of all the K users on the lth subcarrier is made in a parallel way, using the most updated estimation of transmit data symbols to cancel residual interference [46]. This approach results in a less complex system. In figure 2.17, a block model of the implemented system is depicted. It has been shown in [46] that the IB-DFE PIC scheme is very efficient and with a low number of iterations the BER performance is close to the obtained with the matched filter bound, meaning that UTs are efficiently separated while taking advantage of the space-frequency diversity inherent to MIMO SC-FDMA based systems.

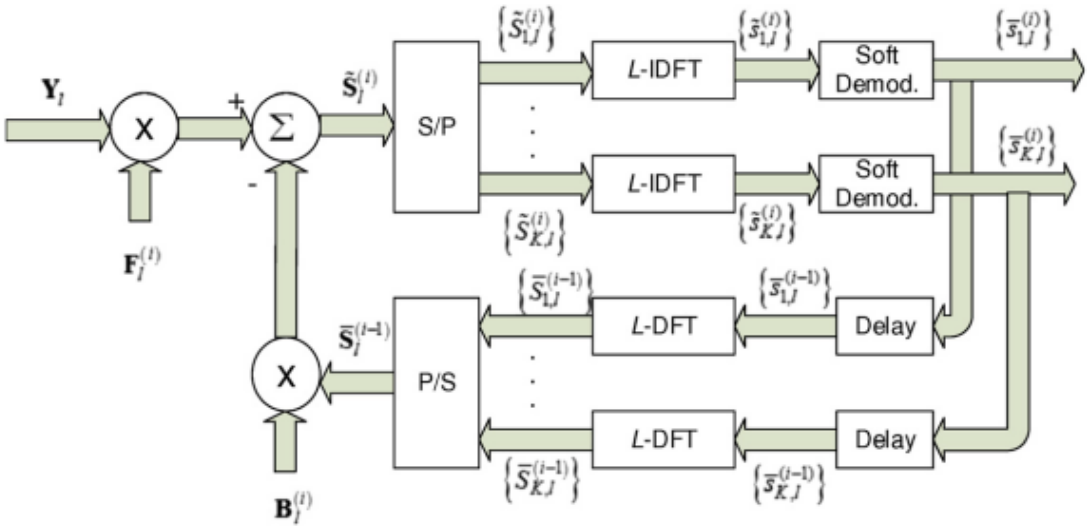

Figure 2.17: Iterative receiver structure based on IB-DFE PIC approach [46]

Considering figure 2.17, for each iteration, after the data is demodulated after the inverse discrete Fourier transform (IDFT) operation is performed, copies of the data pass through a feedback loop where it would be modulated again in order to account for better estimates of the symbols. The feedforward and feedback matrices, respectively $\mathbf{F}_l^{(i)}$ and $\mathbf{B}_l^{(i)}$ are computed in order to minimize the average BER of all UTs and defined by equations 2.5 and 2.7, respectively.

$$\mathbf{F}_l^{(i)} = \left(\mathbf{H}_l^H(\mathbf{I}_K - \mathbf{P}^{(i-1)^2})\mathbf{H}_l + \frac{\sigma_N^2}{\sigma_S^2}\mathbf{I}_M\right)^{-1}\mathbf{H}_l^H\mathbf{\Omega}^{(i)}, \tag{2.5}$$

$$\mathbf{\Omega} = (\mathbf{I}_K - \mathbf{P}^{(i-1)^2}) - \frac{\mu^i}{\sigma_S^2 L}\mathbf{I}_K, \tag{2.6}$$

$$\mathbf{B}_l^{(i)} = \mathbf{H}_l \mathbf{F}_l^{(i)} - \mathbf{I}_K. \tag{2.7}$$

Considering only the first iteration, the matrix $\mathbf{P} = 0$ and thus this equalizer presents a similar performance to conventional linear MMSE equalizers since $\mathbf{B} = 0$ [46].

In [17], a two-step hybrid multi-user equalizer is studied for the receiver structure using an IB-DFE scheme for the digital part, in conjunction with a sub-connected dynamic sub-array. This equalization technique, due to the partial processing in the analogue domain, offers a promising approach for future wireless systems, where reducing costs and power consumption are mandatory.

Chapter 3

Millimeter wave systems and Massive MIMO

The frequency spectrum is a limited resource especially for the current systems. Exploiting milimeter wave(mmWave) technologies, a vast amount of radio frequency spectrum becomes available which can be used to provide greater bandwidth, thus providing higher throughput.

In this chapter the main applications for mmWave communication systems as well as the challenges this technology is facing in order to be deployed for cellular communications are presented. mmWave benefits and limitations are addressed and signal pocessing techniques developed for mmWave communication are also discussed.

3.1 Millimeter wave communications

mmWave systems are characterized mainly by the greater bandwidth availability and the pencil-shaped narrow beams that are transmitted. This opens the door to different applications than the ones usually associated with cellular communications technologies due to the expected reduced size of transceivers. Future use-cases for mmWave can be [47]:

- mmWave communication in wearable devices;
- mmWave communication in virtual reality;
- mmWave communication in vehicular networks;
- mmWave communication in satellite communication;
- mmWave communication in 5G communication systems;
- Object detection, imaging and tracking with mmWave technology;

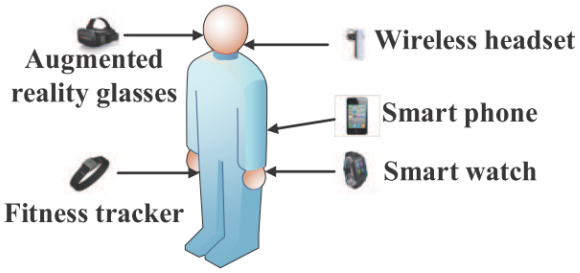

Figure 3.1: Examples of wearable devices around user [47]

Wearable devices, such as fitness tracker, wireless headset, smart watch, smartphone, among others produce massive data traffic, virtual reality headsets also require high data rates in order to offer a more immersive experience that current wireless technologies such as Wi-Fi and Bluetooth cannot provide(current VR headsets are wired to the virtual reality server), such communication systems can be provided by mmWave schemes figure 3.1.

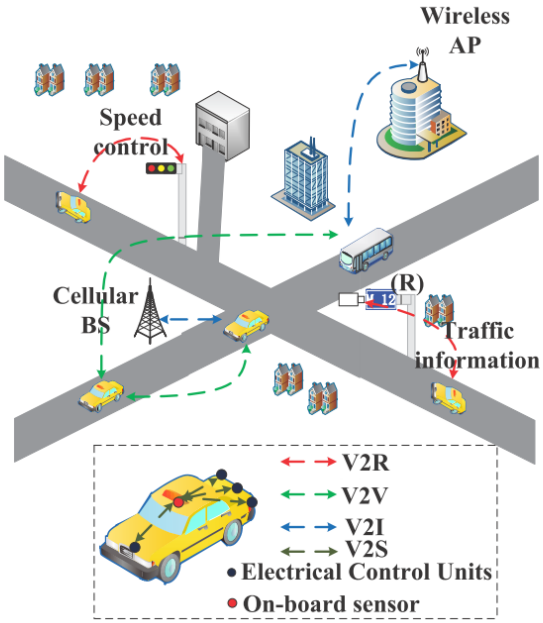

Figure 3.2: Overview of vehicular networks [47]

In vehicular networks mmWave systems can be used for vehicle-to-vehicle, vehicle-to-internet, vehicle-to-road and vehicle-to-sensor communication. These concepts pose great challenges for mmWave systems. The fact that vehicles are moving causes misalignment of the established link between two vehicles, therefore instantaneous driving information should be exchanged in order to construct a robust link between them, thus constructing a vehicular network.

A given vehicle can also be used as a relay to transmit data between two other different vehicles. Vehicles can also connect to road infrastructure in order to exchange relevant traffic

and mobility information, as depicted in figure 3.2 [47].

Regarding object imaging and tracking, the vast majority of mmWave beams can be reflected by objects larger than the wavelength, mmWave systems promise to bring higher accuracy than current microwave systems while at same time can be less expensive, accurate system working at microwave frequencies are costly. A similar paradigm is applicable to object detection, where developments in construction of devices operating at 94 GHz promisse to bring great improvements in detection resolution. Objects as small as a 2.54cm height and radius cilinder can be detected at a distance of up to 60 meters. These systems are particularly useful in monitoring airport runways and high speed roads for 'Foreign Object Debris' which can cause accidents [47] [48].

3.1.1 Spectrum

Almost all mobile/radio communication systems nowadays(cellular, HDTV, satellite communication, GPS and Wi-Fi) use spectrum in the range of 300MHz - 3GHz(figure 3.3), which is an interval already 'crowded' and along with the ever rising number of new devices poses a huge limitation for future wireless communication systems/networks. In order to surpass this spectrum limitation, millimeter wave mobile broadband (MMB) systems are a key technology, allowing exploration of the vast spectrum availability in the range of 3GHz - 300 GHz (wavelength = 100mm to 1mm).

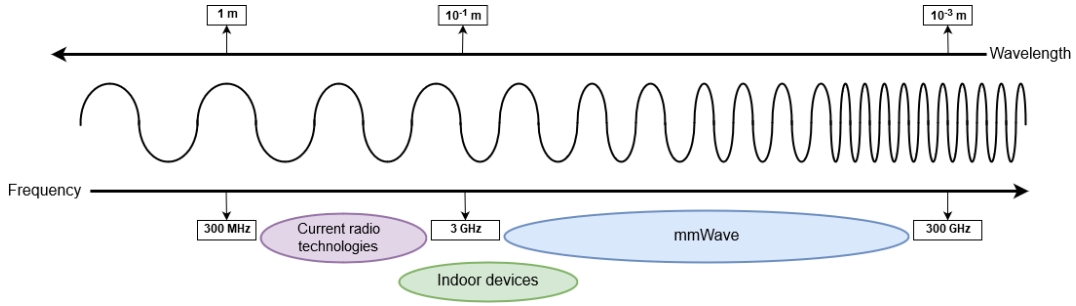

Figure 3.3: Current spectrum allocation

At the ITU World Radiocommunication Conference, global stakeholders are working towards a consensus for spectrum allocation for the IMT-2020 of frequencies within the following ranges: 24.25 – 27.5 GHz, 31.8 – 33.4 GHz, 37 – 40.5 GHz, 40.5 – 42.5 GHz, 42.5 – 43.5 GHz, 45.5 – 47 GHz, 47 – 47.2 GHz, 47.2 – 50.2 GHz, 50.4 GHz – 52.6 GHz, 66 – 76 GHz, and 81 – 86 GHz.

Protocols designed to explore the large bandwidth of mmWave band already exist, capable of achieving very high transmission rates, used in indoor environments. Such cases are the IEEE 802.11n and 802.11ac protocols, which operate at 5GHz, providing significantly higher data rates when compared to other protocols. The first IEEE wireless standard with data rate over 1 Gbps was the 802.15.3c which was capable of multivideo streaming achieving a data rate of 3.8

Gbps. A more recent protocol is the 802.11ad, this protocol was developed in order to achieve multigigabit data rate(up to 7Gbps) on WLANs, operating in the 60 GHz band [49] [50].

3.1.2 Millimeter wave propagation

Regarding free space propagation, despite the fact that waves at higher frequencies propagate less than at lower frequencies, due to smaller wavelength it is possible to pack a higher number of antennas in the same area. This enables transmitter and receiver beamforming (BF) with high gains, in fact if the antenna areas are kept constant there is a gain increase (narrower beam) when compared to conventional systems [51].

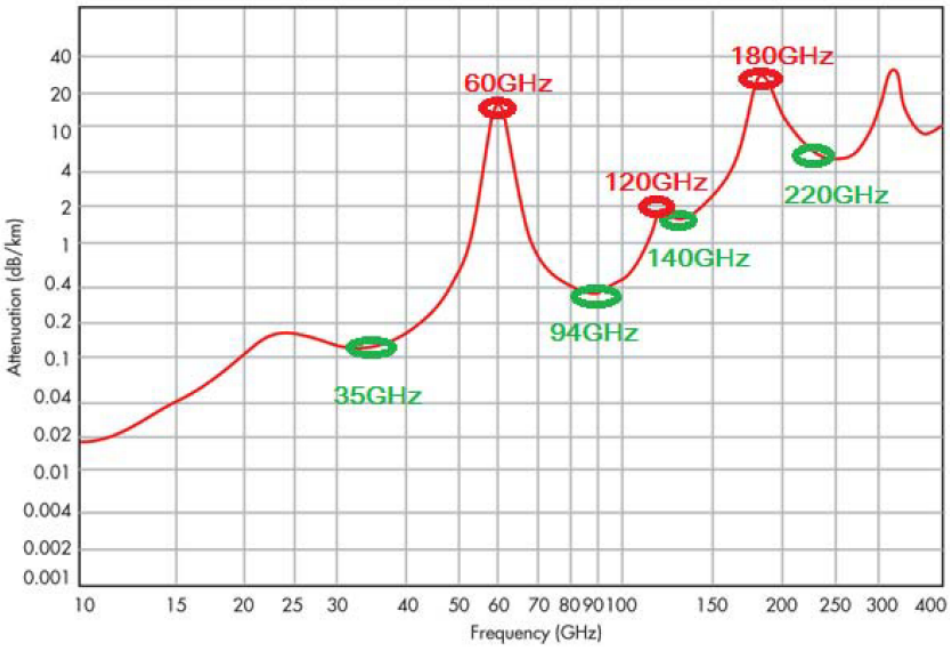

Figure 3.4: Atmospheric and molecular absorption at mmWave frequencies [47]

Even though gaseous losses and precipitation attenuation are typically less than a few dB/Km (except oxygen and water vapor absorption bands) as depicted in figure 3.4, the losses due to reflection and diffraction depend heavily on the material and surface. Although those reduce the range of mmWave, it also facilitates the non line of sight (NLOS) communication, table 3.1 presents the attenuation values of some common materials.

Millimeter wave signals do not penetrate most solid materials effectively, however, some signals might reach inside the building through glass windows and wooden doors. The indoor coverage can also be achieved through the usage of indoor mmWave femto-cells or Wi-Fi solutions. Wi-Fi technology using 60GHz mmWaves is already being developed under IEEE 802.11ad.

Another chalenge for mmWave system is the Doppler shift defined by the following expression, where Δf is the Doppler shift, Δv is the diference in velocity between the BS and the moving

Table 3.1: Attenuation of different materials [52]

		Attenuation (dB)		
Material	Thickness (cm)	<3 GHz	40 GHz	60 GHz
Drywall	2.5	5.4	-	6.0
Office whiteboard	1.9	0.5	-	9.6
Clear glass	0.3/0.4	6.4	2.5	3.6
Mesh glass	0.3	7.7	-	10.2
Chipwood	1.6	-	0.6	-
Wood	0.7	5.4	3.5	-
Plasterboard	1.5	-	2.9	-
Cement	10	-	160	-
Brick wall	10	-	178	-
Concrete	10	17.7	175	-

terminal, c in the speed of light and f_c the carrier frequency:

$$\Delta f = \frac{\Delta v}{c} \times f_c \tag{3.1}$$

The Doppler shift of a wireless channel depends on carrier frequency and mobility, for a carrier frequency of 3-60GHz with terminal mobility of 3-350km/h ranges from 10Hz to 20KHz, additionally the Doppler shift of incoming waves in different angles at the receiver are different, this results in a phenomenon called Doppler spread. When a MMB system is considered, the narrow beams at the transmitter and receiver reduce significantly the angular spread of incoming waves, in turn reducing the Doppler spread. This is expected to cause a much less time-domain variation of an MMB channel when compared to an omnidirectional antenna in a rich scattering environment.

3.1.3 Milimeter-wave mobile broadband network infrastructure

A MMB network consists of multiple MMB base stations that cover a geographic area in order to ensure good coverage. Due to the smaller range of mmWave signals (generally the site-to-site distance as micro- or pico-cell deployment in an urban environment) these would need to be deployed with higher density than current macro-cellular base stations. The transmission and reception in a MMB system are based on narrow beams, suppressing interference from neighbouring MMB base stations and extending the range an MMB link. This allows significant overlap of coverage among neighbouring BSs.

In order to deploy a fully standalone MMB network there are technical constraints that need to be considered: 1) due to high density, the cost to connect every MMB station via wired

network can be significant; 2)low efficiency of radio-frequency devices, such as power amplifiers and multi-antenna arrays.

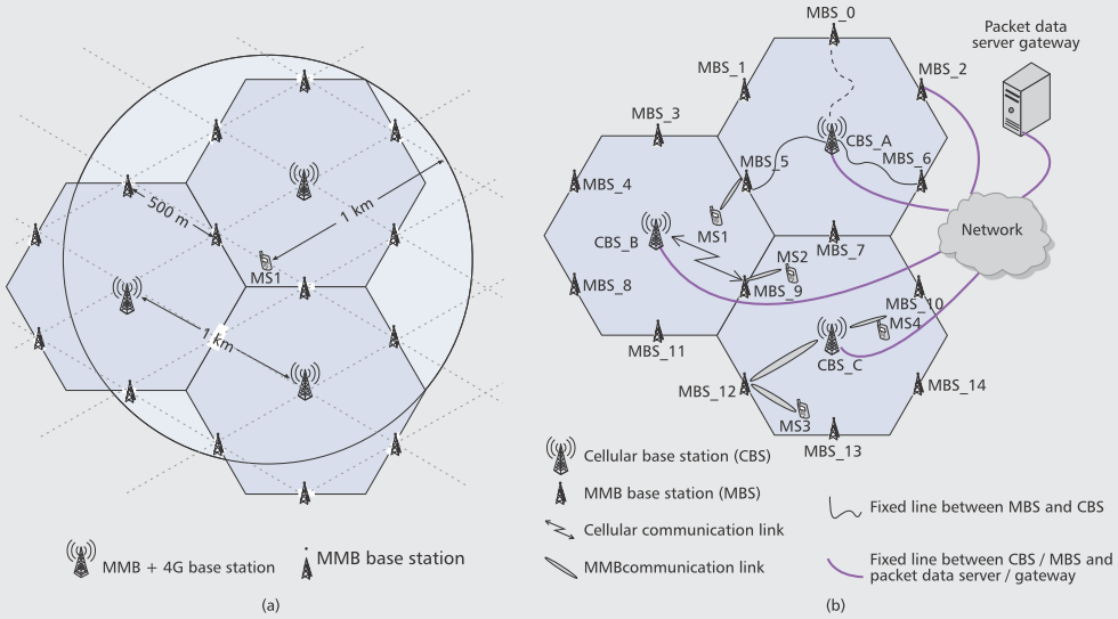

Figure 3.5: Hybrid MMB+4G - architecture and system [52]

A solution that can be more cost- and resource-effective can be the deployment of a Hybrid MMB + 4G system. The already implemented 4G systems are expected to provide good coverage and reliability when MMB systems start to deploy. This can improve coverage and ensure seamless user experience in mobile applications. In a hybrid MMB + 4G system, system information, control channel and feedback are transmitted over the 4G system, allowing for dedicated high data-rate communications over the MMB system [52].

3.1.4 Massive MIMO with millimeter wave

A massive MIMO system is a system which contains a very large number of antennas (counted in the hundreds of antennas) similarly as depicted in figure 3.6. This concept is appealing for 5G and mmWave comunication due to the reduced size of each antenna, typically $\lambda/2$, where λ represents the wavelength in meters. This allows for a high number of antennas to be packed in small areas and yielding significant improvements in capacity gains and energy and spectrum efficiency. The advantages of massive MIMO can be achieved using simple signal processing techniques, such as ZF and MMSE to cope with the channel variability.

Studies [53] show that a user in a massive MIMO system with MMSE and estimated channel state information (CSI) can theoretically achieve the same uplink/downlink throughput using only $\frac{1}{\sqrt{N_t}}$ of the required transmit power if a single antenna would be used. This has implications in terms of design simplicity, cost, efficiency and heat dissipation of the power amplifiers (PAs).

These energy gains can also be used to help overcome the higher path loss at mmWave frequencies and extend the system's operational range.

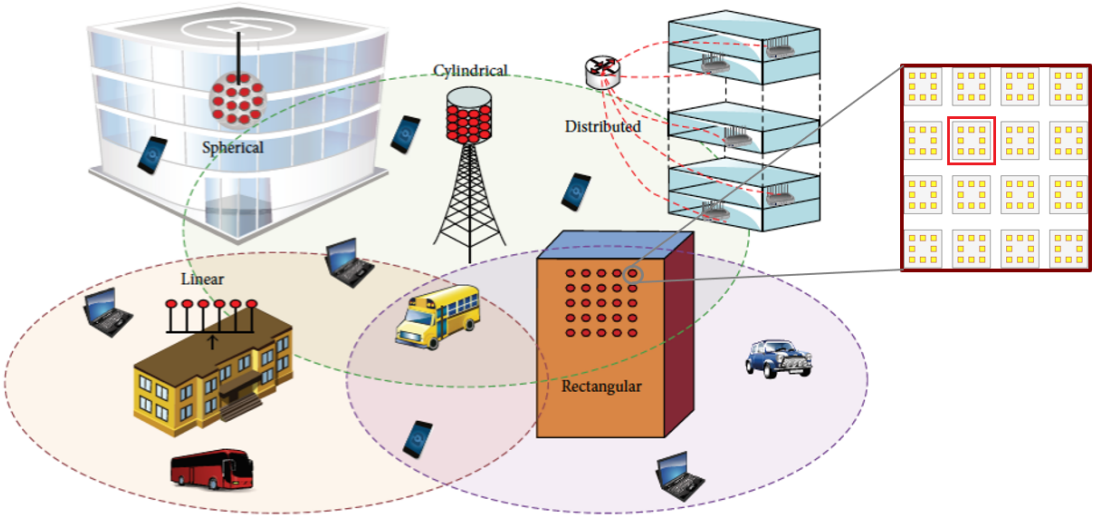

Figure 3.6: Antenna arrays for massive MIMO [54]

Massive mmWave multi antenna systems have a much smaller form factor than designs at current frequencies and would benefit from an increase in available signal bandwidth, additionally, path loss can be beneficial in small-cell scenarios due to limitation of inter-cell interference and allowing greater frequency reuse. Massive MIMO arrays can provide a narrow beam, that would eliminate much of the multipath interference, significantly reducing the delay spread and potentially reducing the need for equalization [55].

3.1.5 Beamforming

High frequency signals, as discussed before, are severely limited due to high propagation losses. Beamforming is a key technology to overcome this limitation. BF is a signal processing technique used for directional signal transmission or reception. When transmitting, a beamformer controls the phase and relative amplitude of the signal at each transmitter antenna to create a pattern of constructive and destructive interference in the wavefront. The massive number of antennas of mMIMO systems will provide significant improvements in terms of beam accuracy and beam steering. Allowing even for two dimensional steering which is a key enabler for mmWave wireless communications. Figure 3.7 shows how the number of antenna sub-arrays employed in the transmission affects the system performance in terms of gain and steerability. For simplicity purpose, it is depicted only one dimension, however, the same principles apply for both vertical and horizontal directions of the antennas.

Considering an antenna array such as the one depicted in figure 3.6 and a sub-array the highlighted zone in the same picture, the array gain is the gain achieved when all sub-array

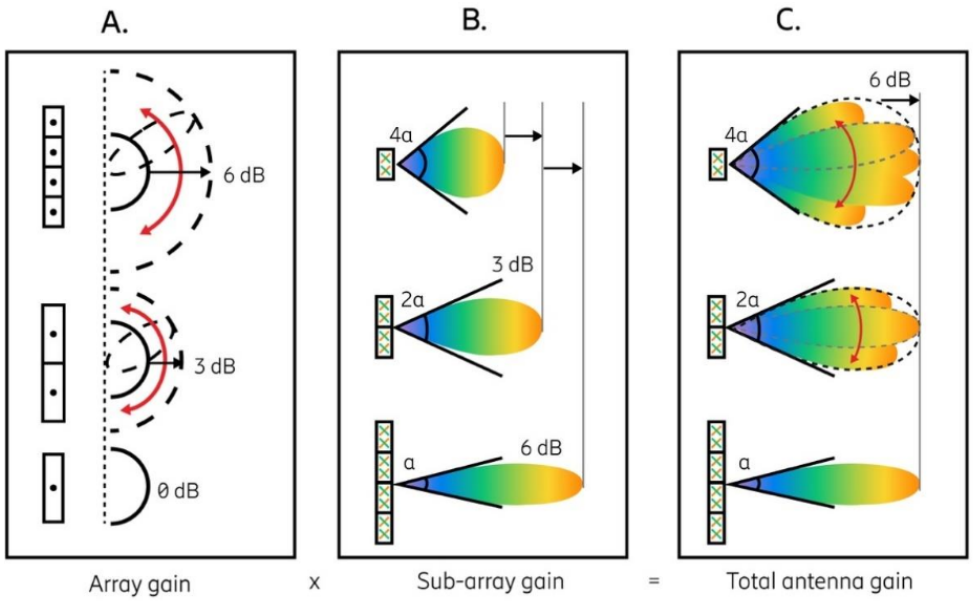

Figure 3.7: Beamforming and beam steering using MIMO [56]

signals are added constructively. The amount of gain relative to one sub-array depends on the number of sub-arrays employed,i.e., two sub-arrays have a gain of 2 (3dB). By adjusting the phase of the sub-array signals in a certain way, this gain can be achieved in any direction as depicted in figure 3.7A. Each sub-array has a characteristic radiation pattern, describing the gain in different directions. The gain and beam width depend on the size of the sub-array. As the size of the sub-array increases, the gain increases and the beamwidth is smaller, as can be seen in figure 3.7B. As depicted in figure 3.7C, the total antenna gain is the product of the previous mentioned gains. The total number of elements determines maximum gain and the sub-array partitioning allows steering of high gain beams over the range of possible directions [56]. Employing beamforming with narrow beams that are highly steerable in a two dimensional space, allows for multilevel sectorization, which is depicted in figure 3.8.

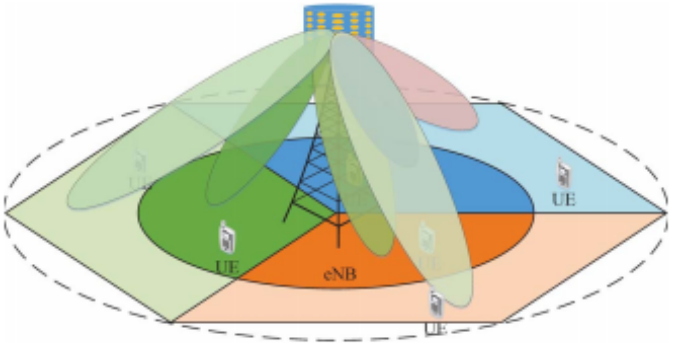

Figure 3.8: BF with multi level sectorization [57]

BF is a key enabling technology for MMB, the small size of the dipoles and separation(both

around $\lambda/2$) of antennas allow a large number of antennas to achieve a high BF gain in a small area. BF can be achieved in both digital and analogue domain, however a pure version of these solutions has either cost or capacity constraints [52]. Pure analog approaches employ a network of digitally controled phase shifters with a single RF chain. Analog BF techniques are limited in terms of precision, making it difficult to finely tune the beams and steer nulls. Other limitation is the poor scalability, since analog BF with a single beamformer only supports single-user and single-stream transmission. In pure digital approaches, each antenna element is connected to a dedicated RF chain, then going through a separate DAC and an ADC. This approach leads to higher precision, however, the need for RF chains equal to number of antenna elements is a major issue due to high cost and power consumption. Hybrid digital-analog BF techniques, that provide the QoS requirements in a more cost effective manner, emerged as a promising solution. These techniques provide a trade-off between low-complexity and high-performance of pure analog and pure digital approaches [47] [52] [58].

Due to the particular characteristics of transmit signals in this band, mmWave channels are expected to be sparse in the angular domain and show less delay spread than current bands channels. Therefore, CSI acquisition is a key aspect in wireless communication systems, specially in mMIMO environments that employ BF. There are two most common methods in order to obtain the downlink CSI and are supported by 5G-NR:

- Reciprocity based CSI – measurements on Sounding Reference Signals (SRS) transmitted by each individual UT;
- Closed loop – UT feedback where the BS transmits CSI-Reference signals which the UTs measure and report back the Pre-Coder Matrix Index which points out the precoder to use out of standardized precoding tables.

In the second method, a beam sweeping transmission procedure is employed. Several synchronization signal blocks(SSB) and reference signals are transmitted, in order to find the best beam direction. In order to create these beams it is required to have a phase calibrated aperture, thus a calibration network is needed in the antenna. The quality of this calibration network will affect the quality of the beams. The UT first determines the best SSB and reports it back to the BS, then, more detailed information can be shared by use of a codebook which will better characterize the CSI. After receiving the estimated CSI from the UT, the BS can select between several beams [56].

3.2 Massive MIMO with Hybrid analog and digital BF

Conventional MIMO systems are based on digital BF. each element in antenna arrays generates one individual RF chain and then goes through a separate ADC and a DAC successively.

This approach may be prohibitive for mmWave since when a large number of antennas are implemented, there is the need for excessive real-time processing as well as high power consumption and high cost if every antenna of the system is required to have a dedicated transceiver [47] [51].

One approach that aims the reduction of total transceivers in a given system is the implementation of analogue BF techniques, where each transceiver is connected to multiple active antennas and the signal phase on each antenna is controlled by a network of analog phase shifters. In analog BF, each transceiver generates one beam toward one user, if the number of users simultaneously served is much smaller than the antenna number (which is held true in most massive MIMO systems), the number of transceivers can be designed to be much smaller than the number of antennas. However, this situation may cause severe inter-user interference in cases when the users are not enough spatially separated, additionally this approach relies on perfect CSI which is hardly the case on mmWave channels due to their high variability. In order to solve this problem, digital BF can be integrated in the system in order to achieve multiple data stream precoding, thus enhancing the overall performance [59].

3.2.1 Hybrid BF structure

Hybrid analog and digital BF is likely the most suited scheme for mmWave communication systems. The core of hybrid BF is to divide precoding between analog and digital domain, making an efficient trade-off between low complexity/limited performance analog BF and high complexity/good performance of fully digital precoding while enaling less RF chains than the number of antenna elements.

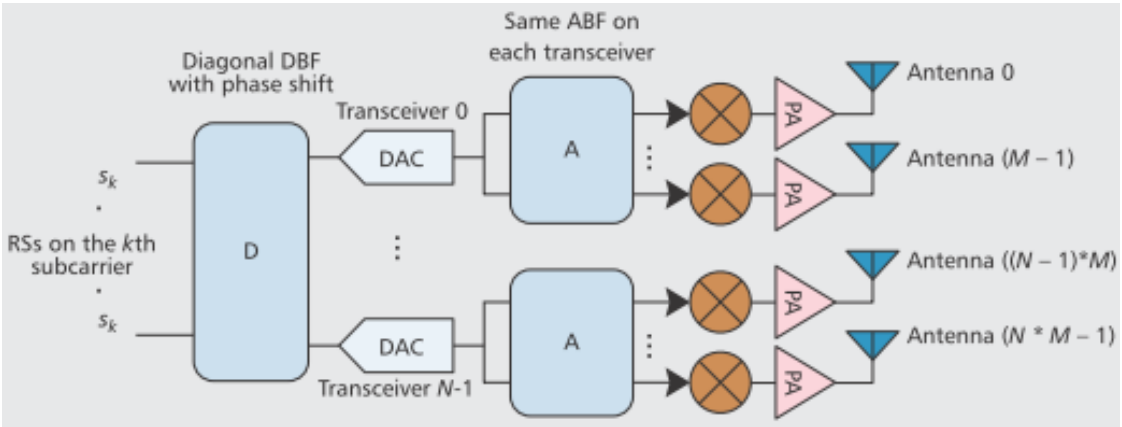

Figure 3.9: $N \times M$ hybrid BF structure [15]

In figure 3.9 is depicted a hybrid analog and digital BF structure. This structure consists of a system with N transceivers, each connected to M antennas. Analog BF is performed over M RF paths in each transceiver, and digital BF is performed over N transceivers. As is demonstrated in [15] that there is a point were the energy efficiency-spectrum efficiency (EE-SE) is maximum,

this point is referred to as the *green point* and can be achieved by adjusting the number of active transceivers as required to guarantee the needed energy-spectrum efficiency [15].

3.3 MIMO precoding and combining in mmWave

Beamforming with multiple data streams, also referred to as precoding, can be done digitally at baseband, in order to further improve mmWave spectral efficiency. It makes a compromise between hardware complexity and system performance by employing large antenna array to achieve high gains with low cost hardware. The small wavelength of mmWave signals allows for a large number of antennas to be packed in relatively small areas and with a small form factor. However, due to the high cost and power consumption of RF chain components such as high resolution ADCs and power amplifiers makes it difficult to have a dedicated RF chain for each antenna. In the current cellular systems, the precoding and combining are performed entirely in the digital baseband. This concept, when applied to massive MIMO becomes infeasible due to hardware constraints, large number of antennas and different channel conditions. New MIMO architectures are needed for mmWave systems. Additionally, in fully analog BF schemes it is difficult to form multiple beams, tune side-lobes and limitation to single stream transmission, due to complexity of implementation of multi-user/stream systems. Two solutions derive from this: 1) hybrid analog/digital precoding and combining, where precoding and BF are divided over different domains, allowing for more degrees of freedom for the precoding design when compared to fully analog schemes; and 2) the use of low-resolution ADCs. This kind of implementation consists of simpler circuitry and less power consumption than high resolution ADC approaches, as the power consumption of these devices increases exponentialy with the resolution [60] [61].

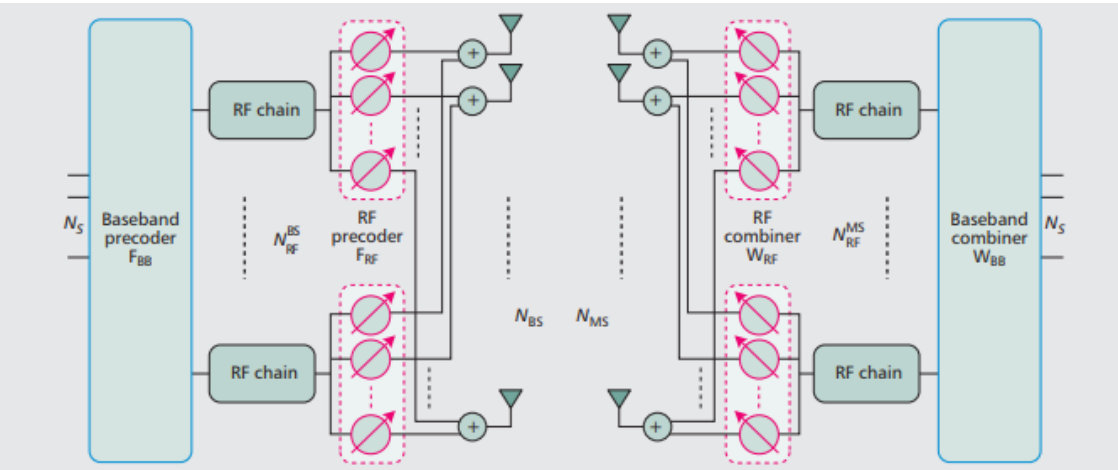

Figure 3.10: Hybrid precoding and combining architecture [60]

3.3.1 Hybrid analog/digital precoding and combining

Hybrid precoding and combining provides a compromise between hardware complexity and performance gain. The number of complete RF chains required is much lower than the number of antennas, making it cost and power efficient. Due to the additional digital layer, hybrid precoding has more freedom in designing the precoding matrices than analog BF. This allows hybrid precoding to perform more complicated processing, and support multi-stream multiplexing and multi-user transmission. It can also enable mmWave systems to perform frequency domain space-time equalization, thus increasing robustness of operation in broadband channels. It can be seen in figure 3.10, a possible implementation of an hybrid precoding and combining scheme, where the number of transmitter/receiver (base station/mobile station) antennas are much larger the the number of RF chains respectively, for each side. Simulations reveal that hybrid precoding and combining has SE ($= 16b/s/Hz$) increase of near 75% when compared to analog BF, approaching the SE of an unconstrained singular value decomposition (SVD) scheme with waterfilling method [60].

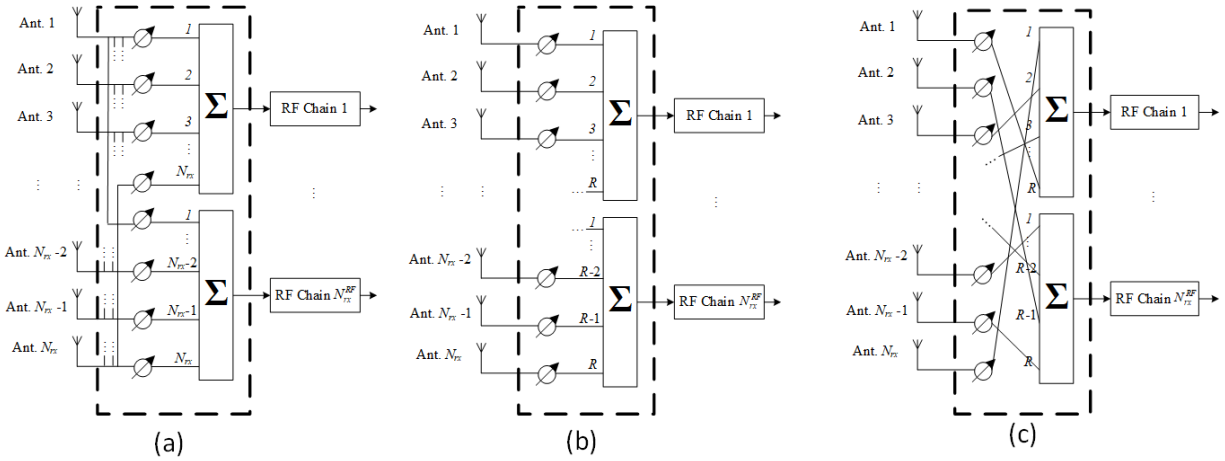

Figure 3.11: Analog part:(a) fully connected;(b) sub-connected with fixed sub-array;(c) sub-connected with dnamic sub-array [17].

There are three different hybrid analog-digital transceiver architectures: fully-connected (depicted in figure 3.10), sub-connected with fixed sub-array and sub-connected with dynamic sub-array. The optimal solution would be the fully-connected architecture. In this system, a given number of RF chains is physically connected to all antennas. This results in a more complex system that requires a very high number of connections, especially if mMIMO is employed. Sub-connected architectures pose a more practical solution for future mmWave broadband systems [62]İn sub-connected architectures, a given RF chain is only connected to a subset of antennas, thus the complexity of this architecture is lower than the fully-connected counterpart. In fixed sub-connected schemes, each RF chain is physically connected to a given subset of antennas. In dynamic sub-connected schemes, each RF chain can be dynamically connected to

different subsets of antennas. The dynamic antenna mapping is derived in order to connect the best set of antennas and phase shifters to each RF chain. This can be done taking into account previous antenna mapping and phase shifter values. In figure 3.11, a comprehensive diagram of the previous structures is drawn. Dynamically sub-connected architectures have shown to outperform fixed sub-connected ones without significant complexity addition. While an acceptable trade-off between performance and complexity happens when comparing to fully-connected schemes. Fixed sub-connected schemes present the worst performance, due to lack of antenna criteria the analog part poorly handles multi-user scenarios [63] [17] [64].

3.3.2 Precoding and combining with low resolution ADC

In conventional MIMO receiver design, the ADCs are expected to have high resolution (6 or more bits), acting as 'transparent' waveform preservers. However, the power consuption of ADCs grows exponentially with the resolution and in mmWave systems the sampling rate of ADCs scales up with the larger bandwidth. Low resolution ADCs have been subject of study in order to implement systems that have much less enegy requirements while providing the requirements of quality of service (QoS) [60].

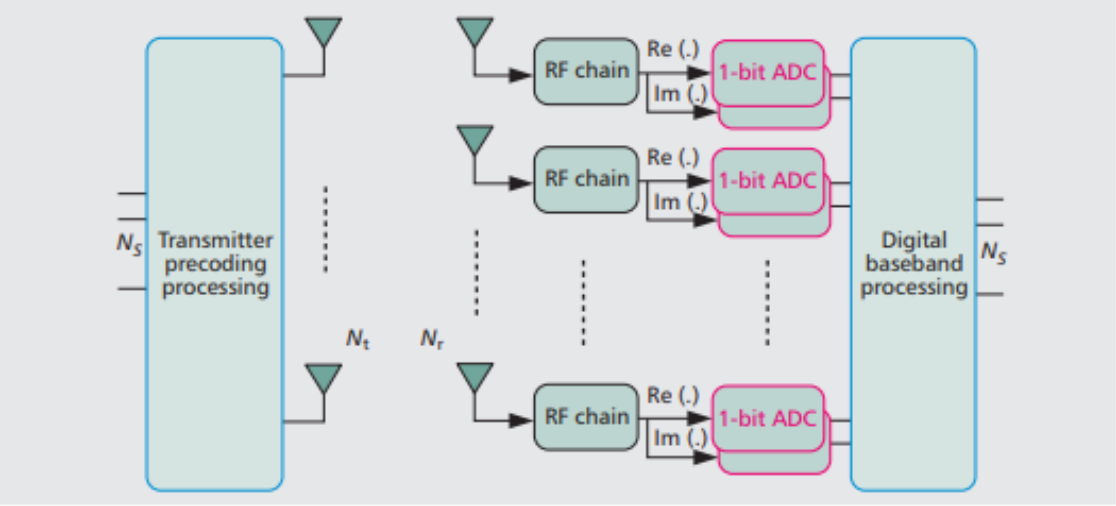

Figure 3.12: System model using 1-bit ADC precoding/combining [60]

In figure 3.12 is depicted a system model using 1-bit ADCs where there is a RF chain and two 1-bit ADCs for each antenna on the receiver. From the transmitter side, the system can be either hybrid precoding, fully digital precoding or analog BF.

There are some disadvantages regarding low resolution ADCs especially 1-bit ADCs, because more RF chains are needed at the receiver. The theoretical capacity achievable is $2N_r$b/s/Hz, being N_r the number of antennas at the receiver (there are only $2N_r$ bits available at the output of the ADCs). However, in order to achieve these gains there are some design challenges to take into consideration when working with 1-bit ADCs, namely the capacity analisys, channel

estimation and broadband channels. Very low quantization methods show a huge performance penalty, however, those can be used for ultra low-power implementations where spectrum efficiency requirements are minor [60].

Chapter 4

Proposed receiver structure for massive MIMO mmWave systems

As previously mentioned, mmWave and mMIMO are two key enabling technologies for 5G. In mmWave bands, several GHz of bandwidth become available, while mMIMO technologies allow for increased throughput and more refined beamforming. The use of multiple sub-arrays in beamforming allows for higher antenna gains, which are a solution to overcome the severe fading effects of mmWave channels. However, conventional MIMO systems employ fully digital architecture, which is not feasible in mMIMO since each antenna would require a dedicated RF chain. Hybrid analog-digital architectures are an option to reduce the number of RF chains per antenna. As the number of antennas grows, there is also an increase in the number of PAs in the system. In order to reduce the costs of operation of future mmWave wireless systems and make its massification feasible, it is of paramount importance that devices have high energy efficiency. The linear PAs used in wireless systems are more efficient when operating close to its saturation zone. This mode of operation causes the PA to behave in a non-linear fashion, thus introducing NLD in the transmitted signals. This NLD can be described analytically, opening the possibility for the BS to have knowledge of the PA characteristics. Therefore, equalization techniques that also take into account the NLD introduced by the PA can be applied on the receiver. The distortion estimates are obtained using a Bussgang receiver and the equalizer is optimized by minimizing the BER, which is equivalent to minimize the mean square error.

This chapter presents the proposed iterative hybrid analog-digital equalizer designed for mMIMO mmWave SC-FDMA systems, under non-linear distortion. The first section contains the characterization of the system. Models of the UTs and BS are presented and are supported by analytical formulation, mmWave channel characterization is also presented. The UTs have low complexity, using a single RF chain connected to multiple phase shifters and antennas. At the base station, an hybrid analog-digital iterative equalizer with fully connected architecture based on IB-DFE principles is implemented in order to eliminate multi-user interference and the

NLD. The second section explains the designed algorithm for signal processing at the receiver. It depicts how data symbols estimates are obtained and later are used to estimate and eliminate the NLD introduced by the PA. Finally, in section 3, the obtained results are presented. The impact that parameters such as the number of users, channel conditions and saturation threshold have in the system performance are also discussed.

4.1 System characterization

The proposed system is an uplink broadband mmWave system, employing hybrid analog-digital equalization with IB-DFE and distortion cancelation on the receiver side. The system has N_c available subcarriers and uses SC-FDMA as the multiple access technique. It is assumed that the system has U UTs sharing the same radio resources and one BS.

In the sections bellow the used models that characterize the proposed system are presented.

4.1.1 Channel model

Regarding the transmission channel, a clustered channel model with N_{cl} clusters and N_{ray} propagation paths per cluster was adopted. For the uth UT, the delay channel matrix $\mathbf{H}_{u,d} \in \mathbb{C}^{N_{rx} \times N_{tx}}$, such that $\mathbb{E}[\| \mathbf{H}_{u,d} \|_F^2] = N_{rx}N_{tx}$ can be expressed as:

$$\mathbf{H}_{u,d} = \sqrt{\frac{N_{rx}N_{tx}}{\rho_{PL}}} \sum_{q=1}^{N_{cl}} \sum_{l=1}^{N_{ray}} \left(\alpha_{q,l}^u p_{rc}(dT_s - \tau_q^u - \tau_{q,l}^u) \times \mathbf{a}_{tx,u}(\theta_q^u - \vartheta_{q,l}^u)\mathbf{a}_{rx,u}^H(\phi_q^u - \varphi_{q,l}^u)\right), \quad (4.1)$$

and in frequency domain at subcarrier k as:

$$\mathbf{H}_{u,k} = \sum_{d=0}^{D-1} \mathbf{H}_{u,d} e^{-j\frac{2\pi k}{N_c}d}. \quad (4.2)$$

The path delays are uniformly distributed in $[0, DT_s]$, where T_s is the sampling interval and D is the cyclic prefix length. The path loss between the UT and BS is ρ_{PL}, while the lth ray in the qth cluster has a complex path gain equal to $\alpha_{q,l}^u$. The function $p_{rc}(.)$ is a rectangular window. The AoA ϕ_q^u and AoD θ_q^u of the qth cluster, and the relative angles of arrival $\varphi_{q,l}^u$ and departure $\vartheta_{q,l}^u$ of the lth ray from the qth cluster have the random distribution presented in [16]. The qth cluster has a time delay τ_q^u and its lth ray has a relative time delay equal to $\tau_{q,l}^u$. The vectors $\mathbf{a}_{rx,u}$ and $\mathbf{a}_{tx,u}$ are the normalizd receive and transmit array response vectors of the uth UT, respectively, and given for an N-element uniform linear array (ULA) by the expression:

$$\mathbf{a}_{ULA}(\theta) = \frac{1}{\sqrt{N}}[1, e^{j2\pi\frac{\gamma}{\lambda}\sin(\theta)}, ..., e^{j2\pi\frac{\gamma}{\lambda}\sin(\theta)(N-1)}]^T, \quad (4.3)$$

where λ and γ are the wavelength and the inter-element spacing, respectively. The channel matrix of the uth UT at the kth subcarrier can be writen as:

$$\mathbf{H}_{u,k} = \mathbf{A}_{rx,u}\mathbf{\Delta}_{u,k}\mathbf{A}_{tx,u}^{H}, \tag{4.4}$$

where the path gains of the lth ray from the qth cluster comprise the diagonal of the diagonal matrix $\mathbf{\Delta}_{u,k} \in \mathbb{C}^{N_{cl}N_{ray} \times N_{cl}N_{ray}}$.

$\mathbf{A}_{tx,u} = [\mathbf{a}_{tx,u}(\theta_1^u - \vartheta_{1,1}^u), ..., \mathbf{a}_{tx,u}(\theta_{N_{cl}}^u - \vartheta_{N_{cl},N_{ray}}^u)] \in \mathbb{C}^{N_{tx} \times N_{cl}N_{ray}}$ and $\mathbf{A}_{rx,u} = [\mathbf{a}_{rx,u}(\phi_1^u - \varphi_{1,1}^u), ..., \mathbf{a}_{rx,u}(\phi_{N_{cl}}^u - \varphi_{N_{cl},N_{ray}}^u)] \in \mathbb{C}^{N_{rx} \times N_{cl}N_{ray}}$ are, respectively, the matrices of the uth user corresponding to the concatenation of all transmit and receive array response vectors.

4.1.2 Transmitter model

Each UT transmits one data stream per subcarrier, number of transmit antennas is denoted as N_{tx}. A block diagram of the uth UT is presented in figure 4.1. It is considered M-QAM constelation, where $s_{u,t}$, t $\in \{1, ..., N_c\}$ denotes a data symbol with $\mathbb{E}[|s_{u,t}|^2] = \sigma^2$ and its DTF is denoted as $c_{u,k}$.

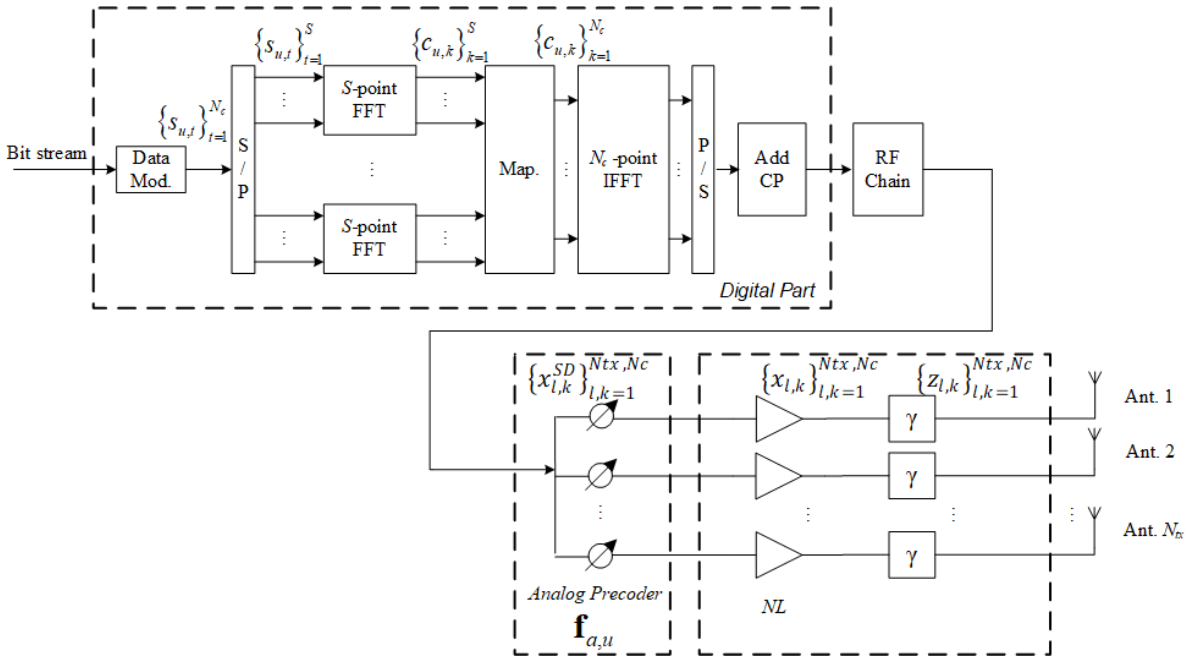

Figure 4.1: Block diagram of the uth UT (transmitter)

After the DFT, the data in the frequency domain are interleaved to increase diversity order and mapped in the SC-FDMA symbol, followed by addition of the CP. Regarding the distortion characterization, the relation between the input and output signals of the PA can be generally obtained for any PA characteristic function. From central limit theorem, the input of the PA device is approximately Gaussian if the number of antennas and/or subcarriers is high. Therefore, from Bussgang's theorem, the output signal can be decomposed into uncorrelated

useful and self-interference components [59], [16]. The PA output in time domain can be written as:

$$\mathbf{x}_{u,t} = \alpha \mathbf{f}_{a,u}.\mathbf{c}_{u,t} + \mathbf{f}_{a,u}\mathbf{d}_{u,t}, \tag{4.5}$$

where α is the multiplication factor of the useful signal component according to the Bussgang theorem [65], $\mathbf{f}_{a,u} \in \mathbb{C}^{N_{tx}}$ is the analog precoder representing the analog phase shifters, $\mathbf{d}_{u,t} \in \mathbb{C}$ is the NLD due to PA,u and t are, the user and time indexes, respectively. The normalized transmitted signal in the frequency domain is given by:

$$\mathbf{x}_{u,k} = f_A(|\mathbf{x}_{u,k}^{SD}|)e^{jarg(\mathbf{x}_{u,k}^{SD})+jf_P(|\mathbf{x}_{u,k}^{SD}|)}, \tag{4.6}$$

which is the derivation of equation 2.3, where $\mathbf{x}_{u,k}$ is the signal plus distortion distortion obtained using Rapp model, $\mathbf{x}_{u,t}^{SD}$ represents the baseband signal without distortion and:

$$\mathbf{z}_{u,k} = \gamma\alpha \mathbf{f}_{a,u}\mathbf{c}_{u,k} + \gamma \mathbf{f}_{a,u}\mathbf{d}_{u,k}, \tag{4.7}$$

where the factor γ is obtained using the equation bellow:

$$\gamma = \frac{E\left[|\mathbf{x}_{u,t}^{SD}|^2\right]}{E\left[|\mathbf{x}_{u,t}|^2\right]}. \tag{4.8}$$

The PA characteristic funtion used in this work is based in the well-known empirical Rapp model, where the AM/AM function is given by 2.4 and the AM/PM function is considered to be zero. The analog precoder $\mathbf{f}_{a,u}$ does not have a subcarrier index because it is constant over all carriers. It was considered an analog precoder, designed in [17], based on the knowledge of partial CSI at the transmitter, i.e., only the average angle of departure (AoD) is assumed to be known at the transmitters. The analog precoder vector of the uth user is given by:

$$\mathbf{f}_{a,u}(n) = \frac{1}{\sqrt{N_{tx}}} exp\{j\arg(\mathbf{\Lambda}_{tx,u}(n,1))\}; n = 1, ..., N_{tx}, \tag{4.9}$$

where $\mathbf{\Lambda}_{tx,u}$ represents the matrix of eigenvalues of the correlation matrix $\mathbf{A}_{tx,u}\mathbf{A}_{tx,u}^H$, i.e. $\mathbf{A}_{tx,u}\mathbf{A}_{tx,u}^H = \mathbf{\Lambda}_{tx,u}\mathbf{\Sigma}_{tx,u}\mathbf{\Lambda}_{tx,u}^H$. $\mathbf{A}_{tx,u}$ is defined by:

$$\mathbf{A}_{tx,u} = [\mathbf{a}_{tx,u}(\phi_{u,1}^{tx}), ..., \mathbf{a}_{tx,u}(\phi_{u,N_{cl}}^{tx})] \in \mathbb{C}^{N_{tx}\times N_{cl}}, \tag{4.10}$$

where $\mathbf{a}_{tx,u}$, u = 1,...,U is the normalized array response vector, which for the ULA case is given by equation 4.3, and $\phi_{u,q}^{tx}$, u=1, q=1,...,N_{cl}, is the average AoD for qth cluster of uth user channel

4.1.3 Receiver model

On the receiver side, the BS has N_{rx} receive antennas and N_{rx}^{RF} RF chains. A fully connected hybrid analog-digital equalizer based on IB-DFE principles with distortion remover block is designed, as depicted in figure 4.2. It is considered that $U \leq N_{rx}^{RF} \leq N_{rx}$.

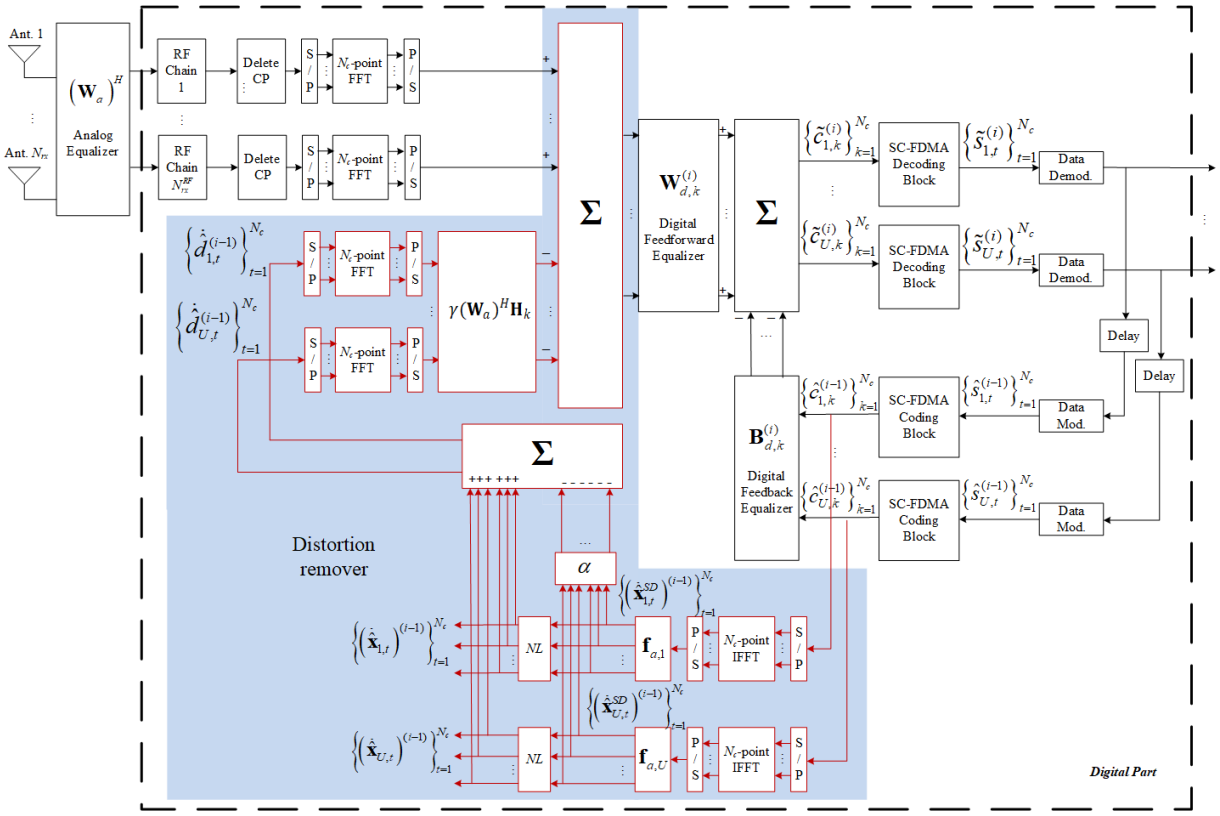

Figure 4.2: Block diagram of the BS (receiver)

The received signal is processed by the analog part through the analog phase shifters, where each element has constant amplitude $|\mathbf{W}_{a_{n,l}}|^2 = N_{rx}^{-1}$, then it is processed over N_{rx}^{RF} RF chains and goes through digital iterative processing composed of a feedback closed loop with forward and feedback paths for each subcarrier. The signal first passes through a linear filter $\mathbf{W}_{d,k}^{(i)}$ at subcarrier k and then follows SC-FDMA decoding and data demodulation. The data recovered from the forward path are modulated and SC-FDMA encoded in the feedback path and sent in two directions, one passes through the feedback filter $\mathbf{B}_{d,k}^{(i)}$, the other is sent to the distortion remover block. In the distortion remover block, represented in figure 4.2 in the blue highlighted zone, the transmitter characteristics are emulated in order to estimate the distortion. This estimation then passes through an equalization block where the analog equalizer $(\mathbf{W}_a)^H$ is applied, as well as the channel characteristic $\mathbf{H}_k$ and the normalization factor γ, after which it is subtracted from the received signal.

The received signal $\mathbf{y}_k$ at the kth subcarrier is given by:

$$\mathbf{y}_k = \sum_{u=1}^{U} \mathbf{H}_{u,k}\mathbf{z}_{u,k} + \mathbf{n}_k, \tag{4.11}$$

where $\mathbf{H}_{u,k} \in \mathbb{C}^{N_{rx}\times N_{tx}}$ is the channel of the uth UT, $n_k \in \mathbb{C}^{N_{rx}}$ the zero-mean Gaussian noise with σ_n^2 variance and $\mathbf{z}_{u,k}$ is the normalized transmitted signal in frequency domain, which, from equations 4.7 and 4.11, further translates into:

$$\mathbf{y}_k = \gamma\alpha \sum_{u=1}^{U} \mathbf{H}_{u,k}\mathbf{f}_{a,u}\mathbf{c}_{u,k} + \gamma \sum_{u=1}^{U} \mathbf{H}_{u,k}\mathbf{f}_{a,u}\mathbf{d}_{u,k} + \mathbf{n}_k, \tag{4.12}$$

where $c_{u,k}$ and $d_{u,k}$ represent, respectively, the estimated data symbols and the estimated distortion value in the kth subcarrier of the uth UT.

Defining $\mathbf{H}_k$ as the overall equivalent channel at kth subcarrier, $\mathbf{H}_k = [\mathbf{H}_{u,k}\mathbf{f}_{a,1}, ..., \mathbf{H}_{U,k}\mathbf{f}_{a,U}] \in \mathbb{C}^{N_{rx}\times U}$, $\mathbf{c}_k = [c_{1,k}, ..., c_{U,k}]^T \in \mathbb{C}^U$ and $\mathbf{d}_k = [d_{1,k}, ..., d_{U,k}]^T \in \mathbb{C}^U$ as the transmitted signal and distortion estimations, respectively, simplifies the above expression into:

$$\mathbf{y}_k = \alpha\gamma\mathbf{H}_k\mathbf{c}_k + \gamma\mathbf{H}_k\mathbf{d}_k + \mathbf{n}_k. \tag{4.13}$$

4.2 Receiver description

The estimated signal at the kth subcarrier and ith iteration, $\tilde{c}_k^{(i)}$, is given by:

$$\tilde{\mathbf{c}}_k^{(i)} = \mathbf{W}_{d,k}^{(i)}(\mathbf{W}_a^H\mathbf{y}_k - \gamma\mathbf{W}_a^H\mathbf{H}_k\hat{\mathbf{d}}_k^{(i-1)}) - \mathbf{B}_{d,k}^{(i)}\hat{\mathbf{c}}_k^{(i-1)}, \tag{4.14}$$

where $\mathbf{B}_{d,k}^{(i)}$ is the digital feedback equalizer matrix of the ith iteration, $\hat{\mathbf{c}}_k^{(i)} = [\hat{c}_{u,k}^{(i)}]_{1\leq u\leq U} \in \mathbb{C}^U$ is the estimate of the transmitted symbols and $\hat{\mathbf{d}}_k^{(i-1)}$ represents the estimated distortion of the kth subcarrier of the $(i-1)$th iteration. This estimation has an associated error such that:

$$\mathbf{d}_k = \hat{\mathbf{d}}_k^{(i-1)} + \hat{\mathbf{d}}_{e,k}^{(i-1)}, \tag{4.15}$$

where $\hat{\mathbf{d}}_{e,k}^{(i-1)}$ represents the error of the distortion estimation. The variance of each of the variables of equation 4.15 are given as follows, $E[\mathbf{d}_k(\mathbf{d}_k)^H] = \sigma_d^2\mathbf{I}_U$, $E[\hat{\mathbf{d}}_k^{(i-1)}(\hat{\mathbf{d}}_k^{(i-1)})^H] = \sigma_d^2(\mathbf{P}_k^{(i-1)})^2\mathbf{I}_U$ and $E[\hat{\mathbf{d}}_{e,k}^{(i-1)}(\hat{\mathbf{d}}_{e,k}^{(i-1)})^H] = \sigma_d^2\big(\mathbf{I}_U(\mathbf{P}_k^{(i-1)})^2\big)$, where $\mathbf{I}_U$ denotes the identity matrix with dimensions $U \times U$ and $\mathbf{P}_k^{(i-1)}$ is defined by equations 4.16 and 4.17.

$$\big(\mathbf{P}_k^{(i-1)}\big)^2 = \mathrm{diag}\big((\rho_{1,k}^{(i-1)})^2, ..., (\rho_{U,k}^{(i-1)})^2\big), \tag{4.16}$$

$$\big(\rho_{u,k}^{(i-1)}\big)^2 = \big|\mathbf{d}_{u,k} - \hat{\mathbf{d}}_{u,k}^{i-1}\big|^2 / \big|\mathbf{d}_{u,k}\big|^2, u \in \{1, ..., S\}, \tag{4.17}$$

The entries of $\mathbf{c}_k = [c_{u,k}]_{1 \leq u \leq U} \in \mathbb{C}^U$ are approximately Gaussian distributed, therefore, the relationship between variables $\mathbf{c}_k$ and $\hat{\mathbf{c}}_k^{(i)}$, $k \in \{1, ..., S\}$ is memoryless. By aplication of the Bussgang theorem [66] it is given by:

$$\hat{\mathbf{c}}_k^{(i)} \approx \mathbf{\Psi}^{(i)} \mathbf{c}_k + \hat{\epsilon}_k^{(i)}, k \in \{1, ..., S\}, \tag{4.18}$$

where $\hat{\epsilon}_k^{(i)}$ is a zero mean vector uncorrelated with $\mathbf{c}_k, k \in \{1, ..., S\}$ and $\mathbf{\Psi}^{(i)} \in \mathbb{C}^{U \times U}$ is a diagonal matrix whose uth element gives a blockwise reliability measure of the estimates of the uth block, associated with the ith iteration. The coeficients of each block are estimated at the receiver computed using equation 4.19,

$$\mathbf{\Psi}_u^{(i)} = \frac{\mathbb{E}[\hat{\mathbf{c}}_k^{(i)}(u)\mathbf{c}_t^*(u)]}{\mathbb{E}[|\mathbf{c}_k(u)|^2]}, u \in \{1, ..., U\}. \tag{4.19}$$

The error between the estimated signal before the S-IFFT, $\hat{\mathbf{c}}_k^{(i)}$ given by equation 4.14 and the transmit signal after S-FFT $\mathbf{c}_k$ is expressed by:

$$\begin{aligned}
\tilde{\epsilon}_k^{(i)} &= \hat{\mathbf{c}}_k^{(i)} - \mathbf{c}_k \\
&= \underbrace{(\alpha\gamma \mathbf{W}_{ad,k}^i \mathbf{H}_k - \mathbf{I}_U - \mathbf{B}_{d,k}^{(i)} \mathbf{\Psi}^{(i-1)}) \mathbf{c}_k}_{\text{Residual ISI}} \\
&- \underbrace{\mathbf{B}_{d,k}^{(i)} \hat{\epsilon}_k^{(i-1)}}_{\text{Errors from estimate } \hat{\mathbf{c}}_k^{(i)}} + \underbrace{\gamma \mathbf{W}_{ad,k}^{(i)} \mathbf{H}_k \hat{\mathbf{d}}_{e,k}^{(i-1)}}_{\text{Errors from estimate } \hat{\mathbf{d}}_k^{(i)}} + \underbrace{\mathbf{W}_{ad,k}^{(i)} \mathbf{n}_k}_{\text{Channel noise}},
\end{aligned} \tag{4.20}$$

where $\mathbf{W}_{ad,k}^{(i)} = \mathbf{W}_{d,k}^{(i)} \mathbf{W}_a^H \in \mathbb{C}^{U \times N_{rx}}$. Observing equation 4.20 one can identify four error terms:

- the residual ISI;
- the error from incorrect estimate of the signal $\mathbf{c}_k$;
- the error from incorrect estimation of the distortion $\mathbf{d}_k$;
- channel noise.

From 4.20 and the properties of the Frobenius norm, we obtain the corresponding mean square error for the kth subcarrier:

$$\begin{aligned}
MSE_k^{(i)} &= \mathbb{E}[\| \hat{\mathbf{c}}_k^{(i)} - \mathbf{c}_k \|^2] = \mathbb{E}[\| \tilde{\epsilon}_k^{(i)} \|^2] \\
&= \| \alpha\gamma \mathbf{W}_{ad,k}^{(i)} \mathbf{H}_k - \mathbf{B}_{d,k}^{(i)} \mathbf{\Psi}^{(i-1)} - \mathbf{I}_U \|_F^2 \, \sigma_u^2 + \| \mathbf{B}_{d,k}^{(i)} (\mathbf{I}_U - |\mathbf{\Psi}^{(i-1)}|^2)^{1/2} \|_F^2 \, \sigma_u^2 \\
&+ \| \gamma \mathbf{W}_{ad,k}^{(i)} \mathbf{H}_k \big(\mathbf{I}_U - (\mathbf{P}_k^{(i-1)})^2\big)^{1/2} \|_F^2 \, \sigma_d^2 + \| \mathbf{W}_{ad,k}^{(i)} \|_F^2 \, \sigma_n^2.
\end{aligned} \tag{4.21}$$

The digital feedback $\mathbf{B}_{d,k}^{(i)}$ and feedforward $\mathbf{W}_{d,k}^{(i)}$ matrices can be designed using the optimization problem given by:

$$\begin{aligned}(\mathbf{W}_{d,k}^{(i)}, \mathbf{B}_{d,k}^{(i)}) \\ &= \arg\min MSE_k^{(i)} \\ &s.t. \sum_{k=1}^{N_c} \mathrm{diag}(\mathbf{W}_{d,k}^{(i)} \mathbf{W}_a^H \mathbf{H}_k) = N_c \mathbf{I}_U, \end{aligned} \tag{4.22}$$

and from Karush-Kuhn-Tucker (KKT) conditions, the solution to the previous problem is:

$$\mathbf{B}_{d,k}^{(i)} = (\alpha\gamma \mathbf{W}_{d,k}^{(i)} \mathbf{W}_a^H \mathbf{H}_k - \mathbf{I}_U)(\mathbf{\Psi}^{(i-1)})^H, \tag{4.23}$$

and

$$\mathbf{W}_{d,k}^{(i)}[\mathbf{W}_a] = \mathbf{\Omega}(\mathbf{H}_k)^H \mathbf{W}_a [(\mathbf{W}_a)^H \tilde{\mathbf{R}}_k^{(i-1)} \mathbf{W}_a]^{-1}, \tag{4.24}$$

where $\mathbf{\Omega}$ and $\tilde{\mathbf{R}}_k^{(i-1)}$ are give by equations 4.25 and 4.26, respectively:

$$\mathbf{\Omega} = \alpha\gamma(\mathbf{I}_U - |\mathbf{\Psi}^{(i-1)}|^2) - \frac{1}{2\sigma_u^2} \sum_{u=1}^{U} \mu_u \mathbf{e}_u \mathbf{e}_u^H, \tag{4.25}$$

$$\tilde{\mathbf{R}}_k^{(i-1)} = (\alpha\gamma)^2 \mathbf{H}_k \big(\mathbf{I}_U - |\mathbf{\Psi}^{(i-1)}|^2\big)(\mathbf{H}_k)^H + \frac{\sigma_n^2}{\sigma_u^2} \mathbf{I}_{N_{rx}} + \frac{\gamma^2 \sigma_d^2}{\sigma_u^2} \mathbf{H}_k \big[\mathbf{I}_U - (\mathbf{P}_k^{(i-1)})^2\big](\mathbf{H}_k)^H. \tag{4.26}$$

Distortion due to the non-linearity added by the PA is obtained based on the Bussgang receiver. The estimated data, without distortion, then passes through a replica of the transmitter, which is the distortion removal block present in figure 4.2. There, the Rapp model is applied in order to estimate distortion present in transmitted signal, from equation 4.5 and considering $\mathbf{f}_{a,u}\mathbf{c}_{u,t} = (\dot{\hat{\mathbf{x}}}_{u,t}^{SD})^{(i-1)}$. This estimation is given by:

$$\dot{\hat{\mathbf{d}}}_{u,t}^{(i-1)} = \dot{\hat{\mathbf{x}}}_{u,t}^{(i-1)} - \alpha(\dot{\hat{\mathbf{x}}}_{u,t}^{SD})^{(i-1)}. \tag{4.27}$$

The associated error with this estimation is given as follows:

$$\dot{\hat{\mathbf{d}}}_{e,k}^{(i-1)} = \mathbf{W}_{d,k}^{(i)}(\mathbf{W}_a \mathbf{y}_k) - \mathbf{W}_{d,k}^{(i)}(\mathbf{W}_a \hat{\mathbf{y}}_k^{(i-1)}), \tag{4.28}$$

where $\hat{\mathbf{y}}_k^{(i-1)}$ is given by:

$$\begin{aligned}\hat{\mathbf{y}}_k^{(i-1)} &= \sum_{u=1}^{U} \mathbf{H}_{u,k} \hat{\mathbf{z}}_{u,k}^{(i-1)} + \mathbf{n}_{e,k} = \\ &= \alpha\gamma \mathbf{H}_k \hat{\mathbf{c}}_k^{(i-1)} + \gamma \mathbf{H}_k \mathbf{d}_k - \gamma \mathbf{H}_k \hat{\mathbf{d}}_{e,k}^{(i-1)} + \mathbf{n}_{e,k}. \end{aligned} \tag{4.29}$$

All the previous steps are synthesized in the below algorithm, where a pseudo-code of the proposed receiver equalized is presented.

Algorithm 1: Receiver algorithm

$\mathbf{\Psi}(0) = 0$;

$\hat{\mathbf{c}}(0) = 0$;

for *i=1* **to** I_{max} **do**

$\mathbf{W}_{d,k}^{(i)} = \mathbf{\Omega}(\mathbf{H}_k)^H \mathbf{W}_a[(\mathbf{W}_a)^H \tilde{\mathbf{R}}_k^{(i-1)} \mathbf{W}_a]^{-1}$;

$\mathbf{B}_{d,k}^{(i)} = (\alpha\gamma \mathbf{W}_{d,k}^{(i)} \mathbf{H}_k - \mathbf{I}_U)(\mathbf{\Psi}^{(i-1)})^H$;

$\tilde{\mathbf{c}}_k^{(i)} = \mathbf{W}_{d,k}^{(i)}(\mathbf{W}_a^H \mathbf{y}_k - \gamma \mathbf{W}_a^H \mathbf{H}_k \hat{\mathbf{d}}_k^{(i-1)}) - \mathbf{B}_{d,k}^{(i)} \hat{\mathbf{c}}_k^{(i-1)}$;

Compute $\mathbf{\Psi}^{(i)}$

$\tilde{\mathbf{R}}_k^{(i)} = (\alpha\gamma)^2 \mathbf{H}_k \big(\mathbf{I}_U - |\mathbf{\Psi}^{(i-1)}|^2\big)(\mathbf{H}_k)^H + \frac{\sigma_n^2}{\sigma_u^2} \mathbf{I}_{N_{rx}} + \frac{\gamma^2 \sigma_d^2}{\sigma_u^2} \mathbf{H}_k \big[\mathbf{I}_U - (\mathbf{P}_k^{(i-1)})^2\big](\mathbf{H}_k)^H$;

$\dot{\hat{\mathbf{d}}}_{u,k}^{(i)} = \dot{\hat{\mathbf{x}}}_{u,k}^{(i-1)} - \alpha(\dot{\hat{\mathbf{x}}}_{u,k}^{SD})^{(i-1)}$;

$\hat{\mathbf{d}}_{e,k}^{(i)} = \mathbf{W}_{d,k}^{(i)}(\mathbf{W}_a \mathbf{y}_k) - \mathbf{W}_{d,k}^{(i)}(\mathbf{W}_a \hat{\mathbf{y}}_k^{(i-1)})$;

end

4.3 Results

This section presents the main results obtained for the proposed model. For each UT, a wideband mmWave channel model (4.1) with $N_{cl} = 12$ clusters, each one with $N_{ray} = 10$ rays is considered; the number of considered users is $U = 8$. As in [16] the azimuth AoD and AoA have Laplacian distribution, and the complex path gain of the lth path of the qth cluster $\alpha_{q,l}^u$ is a random complex Gaussian variable. The angle spread for both transmitters and receiver are set to 10 degrees. It is assumed that the average power for all $N_c l$ clusters is the same and that the path delays have a uniform distribution in the CP interval. Additionaly it is considered that the antenna element spacing if half-wavelength with carrier frequency equal to 72 GHz and that all the UTs and the BS employ ULAs.

The system has $N_{tx} = 16$ transmit antennas and $N_{rx} = 128$ receiver antennas, it supports $N_c = 512$ subcarriers and a CP of length $D = N_c/4 = 128$. The length of each detected block at the BS is $S = 128$, QPSK modulation is adopted. All simulations employ the Monte Carlo method.

Table 4.1: Simulation parameters

Parameter	**Value**
Carrier frequency	72 GHz
Antenna element spacing	Half-wavelength
Array configuration	ULA
Decay from the first to the last channel cluster	10 dB
Decay from the first to the last ray of each channel cluster	10 dB
N_{cl}	12
N_{ray}	10
Angle spread, σ	10°
N_c	512
FFT size	256
D	$N_c/4$
U = N_{rx}^{RF}	8
N_{tx}	16
N_{rx}	128

Two distinct scenarios are considered in this section. As depicted in table 4.2, the first scenario, A, it is considered for 8 users, $N_{cl} = 12$ clusters and $N_{ray} = 10$ rays for various values of the saturation threshold s_M. In the second scenario, B, the number of clusters is set to $N_{cl} = 4$ and $N_{ray} = 5$ rays for different numbers of users. In this scenario comparisons are made for the case when $s_M = 0.8$ and the ideal PA. Performance analysis is performed by mean of the bit error rate (BER) as a function of the ratio of average bit energy and the one-sided noise power spectral density, i.e., E_b/N_0.

Table 4.2: Parameter values for simulated scenarios

	Parameter		
Scenario	Users	N_{cl}	N_{ray}
A	8	12	10
	4	12	10
B	8	4	5
	4	4	5
	16	4	5

4.3.1 Scenario A

Figures 4.3,4.4 and 4.5 present the curves obtained of BER as a function of E_b/N_0 for each iteration, for different values of the saturation threshold $s_M = [0.5, 0.8, 1.1]$, as well as the curve obtained for the case when an ideal PA is considered, for comparison.The maximum number of iterations considered is $I = 10$.

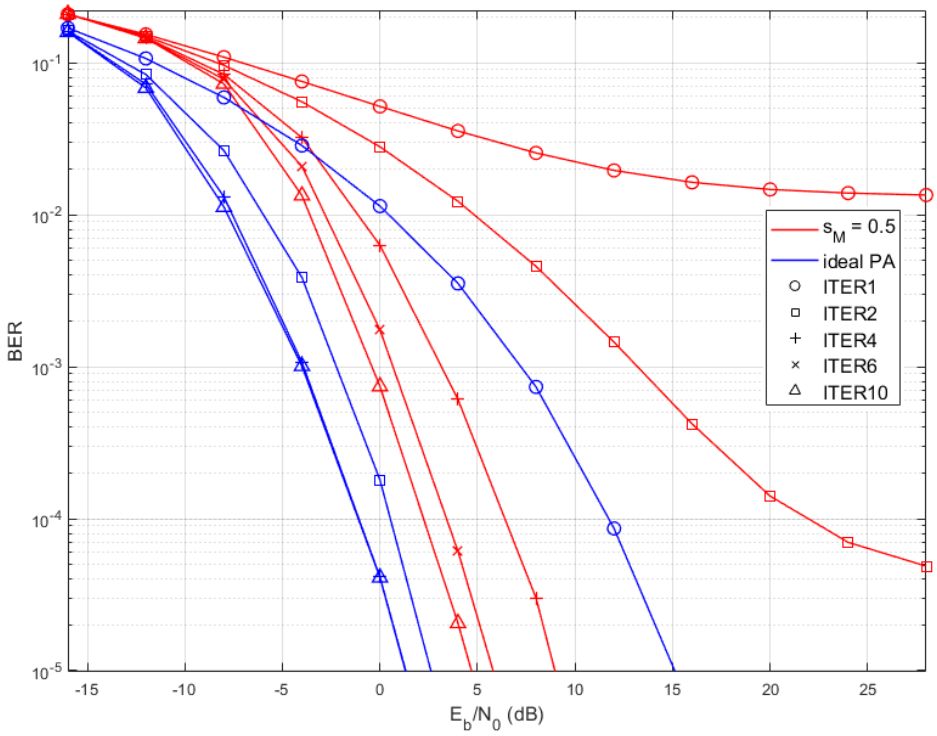

Figure 4.3: Performance of the proposed equalizer for 8 users and $s_M = 0.5$

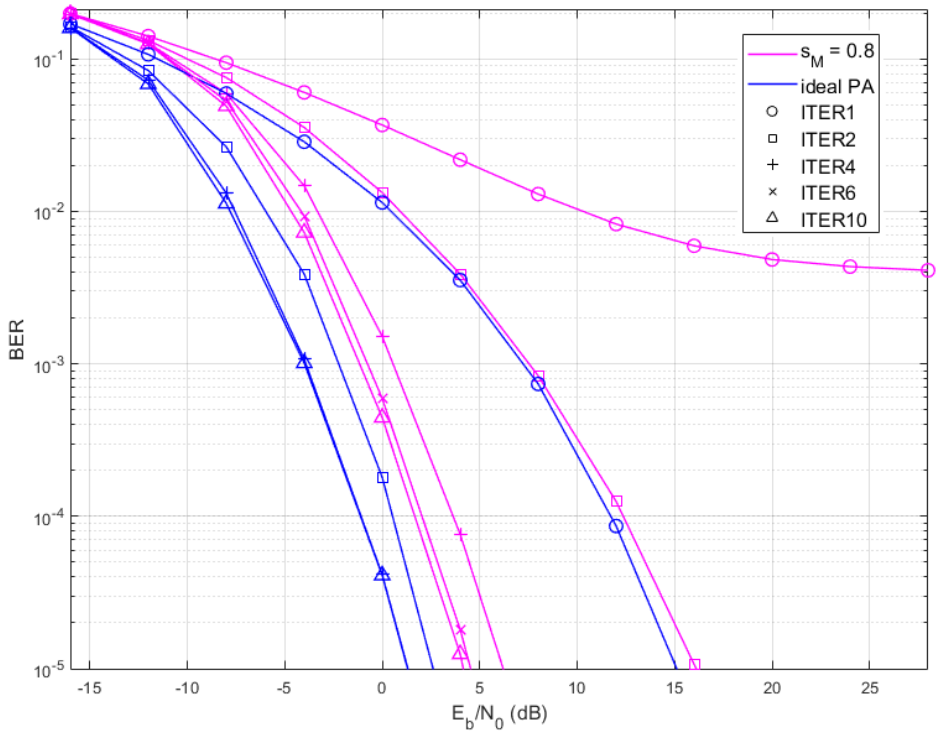

Figure 4.4: Performance of the proposed equalizer for 8 users and $s_M = 0.8$

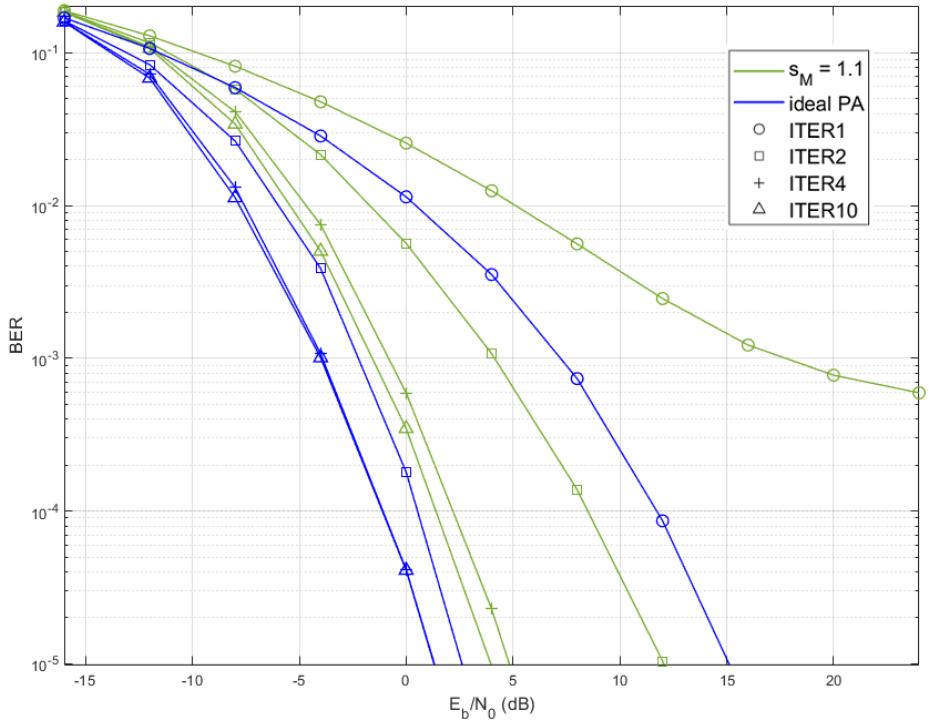

Figure 4.5: Performance of the proposed equalizer for 8 users and $s_M = 1.1$

As can be observed in figures 4.3 to 4.5 the system is able to effectively reduce the effects of both multi-user interference and NLD caused by the amplifier and cope with the saturation

of the PA, thus increasing performance. In the case when an ideal PA is considered, with just four iterations it is achieved a performance with residual difference to when ten iterations are performed. In this case, for a BER target of 10^{-3}, a gain of 11 dB E_b/N_0 can be achieved comparatively to the first iteration case. Considering the PA NLD, it can be observed a great performance penalty when compared to the ideal PA case, it is visible that, for small number of iterations (two or less) the BER decreases asymptotically as E_b/N_0 increases, which happens due to PA saturation. Nevertheless, after some iterations the system is able to compensate the distortion and achieve performances comparable to the ideal PA,with less than 5 dB penalty when 10 iterations are performed.

Observing the above figures it is noticeable that the greater improvements in the system performance occur in the first four iterations. Except when $s_M = 0.5$ the difference between the fourth and tenth iterations is less than 3 dB. After 10 iterations all the above considered cases achieved the BER goal of 10^{-3} with $E_b/N_0 \leq 0$ value.

Figure 4.6 presents a performance comparison between the previous simulated scenarios. It presents the required E_b/N_0 to achieve a BER of 10^{-3} as a function of the number of iterations, considering 8 users. Results for the 1st iteration for the cases when $s_M = [0.5, 0.8]$ are omitted because the required BER value is not achieved. As expected, as the PA saturation region decreases, the impact of NLD on the system performance increases. However this difference diminish whit the number of iterations.

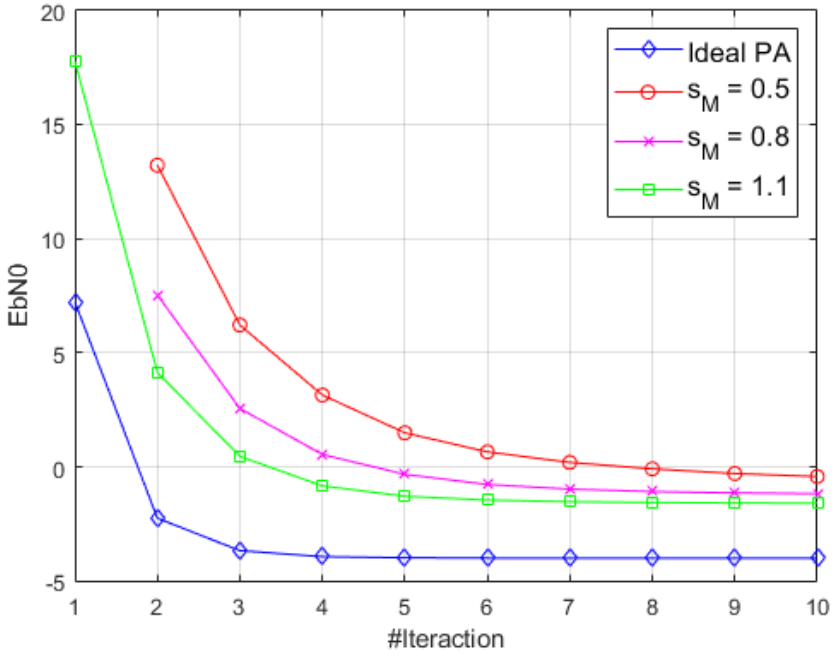

Figure 4.6: Performance of E_b/N_0 as function of the number of iterations

It is noticeable that the difference in performance between the 6th and 10th iterations is

somewhat negligible, and when $s_M = [0.8, 1.1]$, there is less than 1 dB penalty to achieve the same BER as when 10 iterations are performed. Thus, is possible to conclude that 6 iterations is enough to take the maximum advantages of the proposed algorithm.

Figure 4.7 presents the required E_b/N_0 to achieve the BER goal of 10^{-3} as a function of the saturation threshold, for each selected iteration. The impact of s_M on the system performance is evident, especially with low number of iterations. If only two iterations are performed, there is a 10 dB difference between the cases when $s_M = 0.5$ and $s_M = 1.1$. The performance difference becomes less evident if more iterations are performed.

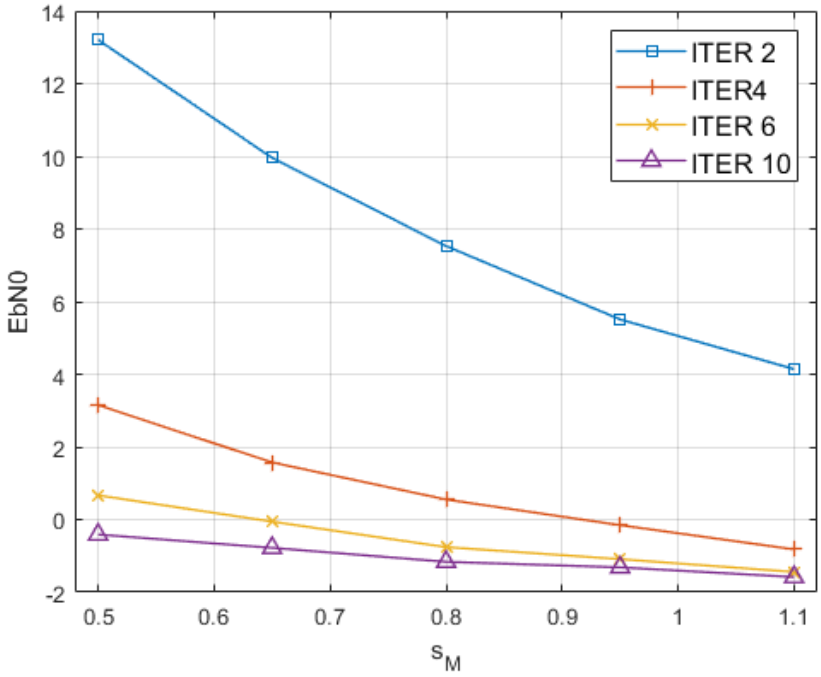

Figure 4.7: Required EbN0 to achieve target BER as function of s_M for each iteration

When a higher number of iterations is performed, the impact of s_M in the system performance is greatly reduced, almost negligible. If ten iterations are performed, there is a less than 2 dB of difference between the best and the worst considered s_M values. This demonstrates that the proposed system is able minimize the impact of the PA characteristics or the operation region in the overall performance of the system.

Figure 4.8 presents the results obtained for the cases when 8 and 4 users are considered. As expected, when 8 users are considered, the system performs better. The performance penalty due to reducing the number of users is clearly visible, and it increases as more iterations are performed. If ten iterations are performed, there is a 5 dB penalty in performance. This happens because with 8 users, the estimations of the distortion are more accurate, thus the distortion is removed more effectively.

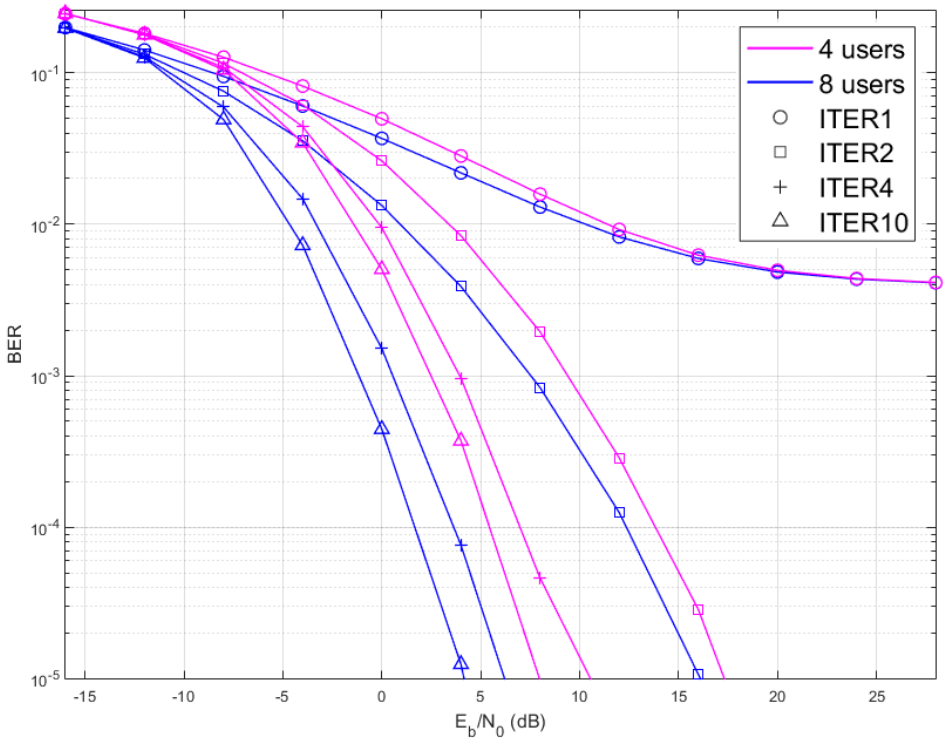

Figure 4.8: Performance comparison between 8 and 4 users for $s_M = 0.8$

4.3.2 Scenario B

For this scenario the value of the saturation threshold $s_M = 0.8$ was fixed as well as $N_{cl} = 4$ clusters and $N_{ray} = 5$ rays. Figures 4.9,4.10 and 4.11 present comparison in performance between the cases where we have NLD due to PA and the ideal PA. Both cases were considered with 4, 8 and 16 users and are depicted in figures 4.9, 4.10 and 4.11, respectively.

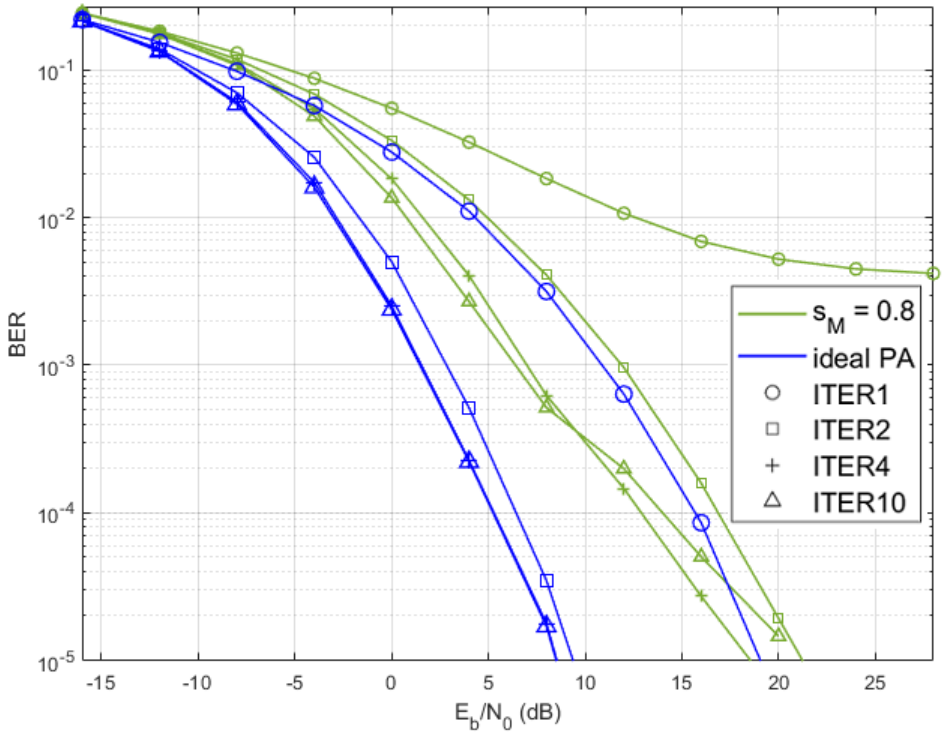

Figure 4.9: Performance of the proposed equalizer for 4 users and $s_M = 0.8$

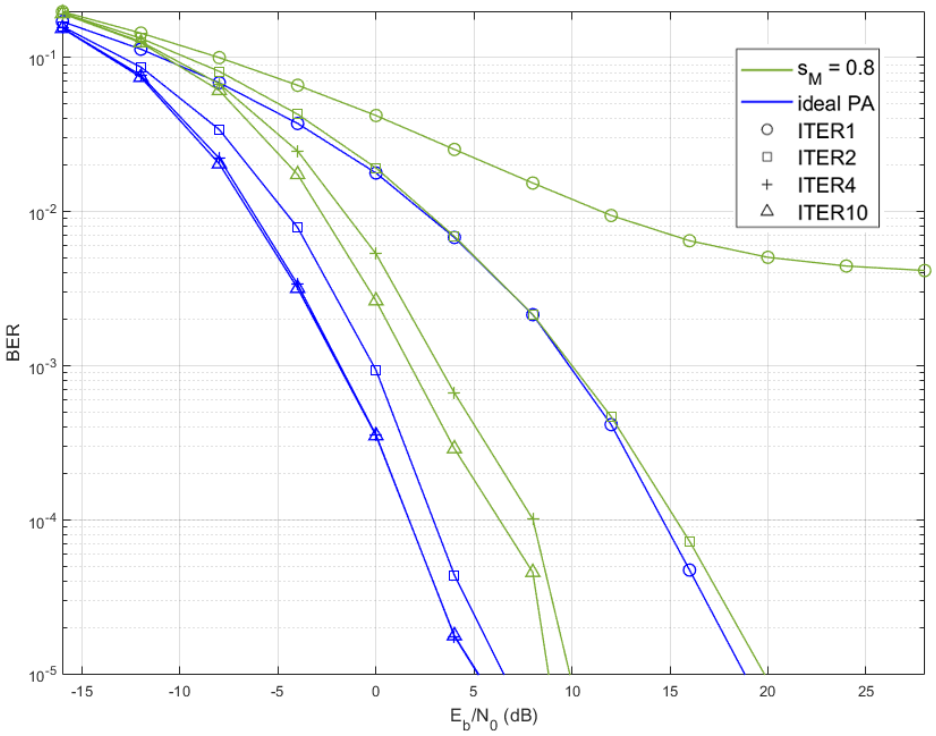

Figure 4.10: Performance of the proposed equalizer for 8 users and $s_M = 0.8$

Observing the above figures, is visible that the tendency of the previous scenario is still present, BER performance increases with the number of users. The performance penalty is also roughly the same, with a 5 dB penalty to achieve target BER when ten iterations are considered.

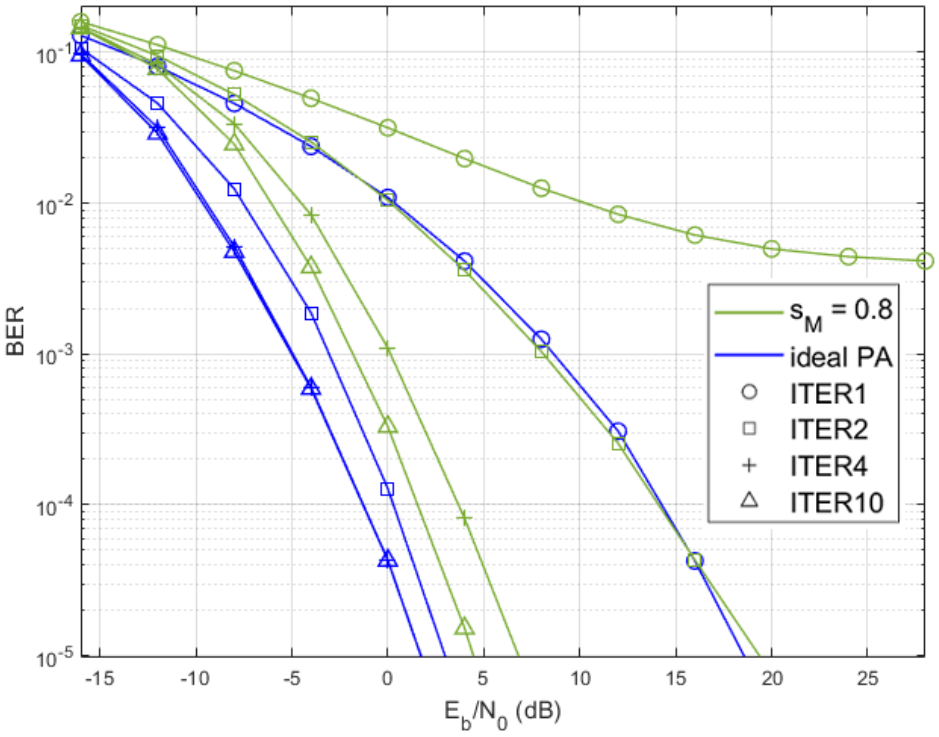

Figure 4.11: Performance of the proposed equalizer for 16 users and $s_M = 0.8$

If 16 users are considered, the BER improvement relatively to the case with 8 users is 4 dB. It is noticeable, for the results presented in this scenario, a large performance penalty due to the reduction in the number of clusters and rays. This reduction in N_{cl} and N_{ray} is characteristic of adverse channel conditions when just a few reflections are effectively received. However, the system performs better as the number of users increases. The BER is lower as the number of connected users increases because the BS can gather more information on the IB-DFE and distortion remover block. In this way, better estimates are computed regarding user interference and NLD. In this way the negative impacts of these effects are mitigated, thus increasing the effectiveness of the system.

Chapter 5

Conclusion and future work

Wireless communication systems are constantly evolving. From analog technology to LTE, the continuous improvement is driven by the necessity to meet more demanding requirements. In order to achieve the proposed requirements for 5G, the need to exploit higher bands of the electromagnetic spectrum arises and the mmWave band provides a good opportunity for this new leap in wireless communications. The vast amount of available spectrum is key to provide the large bandwidth necessary to meet the required QoS for 5G. Additionally, as the carrier frequency increases, the number of antennas that can be packed in the same area also increases, making mMIMO and mmWave key enabling technologies for future multi-Gbps wireless communications. However, these new technologies also imply certain limitations and hardware constraints, as the number of cells drastically increases, an inevitability due to poor propagation inherent to higher frequency operation, it is important that each network device is as energy efficient as possible with minimal impact on the overall performance of the system. The scope of this dissertation was to present a new hybrid equalizer solution that takes into account the NLD introduced by the PAs. The system has low complexity and enables energy efficiency requirements of 5G without compromising throughput.

5.0.1 Conclusions

This dissertation started with the presentation of an overview of the evolution of wireless communications culminating in the future generation of telecommunication systems, the 5G. A brief discussion regarding the key paradigms of the 5G and future wireless communication systems is addressed in the first chapter. The pace at which telecommunication systems evolved is truly remarkable. In just forty years, cellular systems went from bulky, analog, voice transmission only equipment to digital, multifunctional, lightweight and powerful smartphones which comprise the whole world in the palm of a hand.

The second chapter presents a theoretical analysis of single-carrier and multi-carrier modulation schemes, power amplification and NLD that derives from it. Concepts such as multiple

antenna systems, equalization and interference cancellation are also discussed as those are essential for the development of this dissertation.

The third chapter addressed the mmWave communication technology. Specific aspects of this technology are presented, such as the vast availability of electromagnetic spectrum and the characteristic attenuation in mmWave propagation are presented. New technologies that derive from mmWave, such as massive MIMO due to the small size of antennas and beamforming are also discussed, as well as new transceiver structures to cope with the specific characteristics that operation at mmWave requires.

In the fourth chapter, the designed receiver structure is presented. The proposed system consists of an uplink broadband mmWave system, employing hybrid analog-digital equalization based on the IB-DFE principles and distortion cancellation on the receiver side. The receiver, transmitter and mmWave channel model were described in this chapter. The impact of NLD on the BER performance of the presented system was presented. The distortion estimation was obtained based on a Bussgang receiver. It was observed that, under different conditions, the proposed equaliser was able to effectively compensate the NLD and improve the BER after some iterations. It was also noticeable the performance increases with the number of users, since the equalizer could gather more information of the NLD and eliminate distortion more effectively. The main conclusions that derive from this dissertation are:

- The proposed hybrid analog-digital equalizer with IB-DFE and distortion cancellation scheme provides a significant improvement in the BER performance with just a few iterations. This is verified because most of the multi-user interference and distortion are removed in the 1st to 2nd iterations;
- The BER performance increases as the saturation threshold is higher. At higher saturation thresholds is less likely that the PA will enter deep saturation mode, thus less distortion is introduced in the signals;
- As the number of users increases, the BER decreases. This happens because the BS can collect more information, thus compute better estimates of the data.
- The BER also decreases with an increase in number of N_{ray} and N_{cl} showing that the system performs better in an environment with multiple reflections. This is due increased diversity gains, thus mitigating NLD and multi-user interference;

5.0.2 Future work

To conclude this dissertation, some suggestions regarding future work are presented. In this work, a few assumptions were made regarding the proposed system. In this dissertation, the UTs transmit only one data stream, future work may include transmission of multiple data streams.

In addition, the precoder algorithm employed in the transmitter, i.e. the UT, is based on average angle of departure, other precoder schemes can be tested to further access the robustness of the proposed equalizer. Finally, the equalizer presented in this work is based on a fully connected hybrid analog-digital architecture, where each RF chain is physically connected to all antennas, thus requiring a large number of connections for a large number of antennas and/or high number of RF chains. Therefore a similar implementation using sub-connected or partially connected architecture would be of interest due to increased simplicity for development of real systems.

Bibliography

[1] A. Rees, *The cyclopaedia; or, Universal dictionary of arts, sciences, and literature. Plates.* London Longman, Hurst, Rees, Orme & Brown, 1820.

[2] "Mark V military heliograph,1940." https://www.vanleestantiques.com/product/mark-v-military-heliograph1940/.

[3] R. Wenzlhuemer, *Connecting the Nineteenth-Century World: The Telegraph and Globalization.* Cambridge University Press, 2013. Google-Books-ID: jLgBnwEACAAJ.

[4] "Morse Key - Marconi's Wireless Telegraph, circa 1905." https://collections.museumvictoria.com.au/items/404170.

[5] "List of Marconi wireless stations - Wikiwand." https://www.wikiwand.com/en/List_of_Marconi_wireless_stations.

[6] "From Backpack Transceiver to Smartphone: A Visual History of the Mobile Phone." https://smartphones.gadgethacks.com/news/from-backpack-transceiver-smartphone-visual-history-mobile-phone-0127134/.

[7] V. Pereira and T. Sousa, "Evolution of Mobile Communications: from 1g to 4g." http://infoboxdaily.com/wp-content/uploads/2014/10/eden.dei.uc.pt_~vasco_Papers_files_Mobile_evolution_v1.5.1.pdf.

[8] "1g, 2g,... & 5g: The evolution of the G's | MS&E 238 Blog." https://mse238blog.stanford.edu/2017/07/ssound/1g-2g-5g-the-evolution-of-the-gs/.

[9] S. M. Tondare, S. D. Panchal, and D. T. Kushnure, "Evolutiontuonary steps from 1g to 4g." https://ijarcce.com/wp-content/uploads/2012/03/IJARCCE1C-a-Sachin-Panchal-Evolutionary-steps.pdf, 2014.

[10] "Global statistics." https://www.5gamericas.org/resources/charts-statistics/global/.

[11] P. Demestichas, A. Georgakopoulos, D. Karvounas, K. Tsagkaris, V. Stavroulaki, J. Lu, C. Xiong, and J. Yao, "5g on the Horizon: Key Challenges for the Radio-Access Network," *IEEE Vehicular Technology Magazine*, vol. 8, pp. 47–53, Sept. 2013.

[12] "Promoting the shared use of Europe's radio spectrum." `https://ec.europa.eu/digital-single-market/en/promoting-shared-use-europes-radio-spectrum`, Oct. 2012.

[13] "IMT traffic estimates." `https://www.itu.int/dms_pub/itu-r/opb/rep/R-REP-M.2370-2015-PDF-E.pdf`.

[14] "Ericsson Mobility Report November 2019," p. 36, 2019.

[15] S. Han, C.-l. I, Z. Xu, and C. Rowell, "Large-scale antenna systems with hybrid analog and digital beamforming for millimeter wave 5g," *IEEE Communications Magazine*, vol. 53, pp. 186–194, Jan. 2015.

[16] A. Alkhateeb and R. W. Heath, "Frequency Selective Hybrid Precoding for Limited Feedback Millimeter Wave Systems," *IEEE Transactions on Communications*, vol. 64, pp. 1801–1818, May 2016.

[17] R. Magueta, D. Castanheira, A. Silva, R. Dinis, and A. Gameiro, "Hybrid Multi-User Equalizer for Massive MIMO Millimeter-Wave Dynamic Subconnected Architecture," *IEEE Access*, vol. 7, pp. 79017–79029, 2019.

[18] R. Magueta, D. Castanheira, A. Silva, R. Dinis, and A. Gameiro, "Hybrid Iterative Space-Time Equalization for Multi-User mmW Massive MIMO Systems," *IEEE Transactions on Communications*, vol. 65, pp. 608–620, Feb. 2017.

[19] D. Zhu, B. Li, and P. Liang, "A Novel Hybrid Beamforming Algorithm With Unified Analog Beamforming by Subspace Construction Based on Partial CSI for Massive MIMO-OFDM Systems," *IEEE Transactions on Communications*, vol. 65, pp. 594–607, Feb. 2017.

[20] S. Park, J. Park, A. Yazdan, and R. W. Heath, "Exploiting Spatial Channel Covariance for Hybrid Precoding in Massive MIMO Systems," *IEEE Transactions on Signal Processing*, vol. 65, pp. 3818–3832, July 2017.

[21] S. Teodoro, A. Silva, R. Dinis, and A. Gameiro, "Performance Impact of Nonlinear Amplification in Massive MIMO mmWave Systems," in *2019 IEEE 89th Vehicular Technology Conference (VTC2019-Spring)*, (Kuala Lumpur, Malaysia), pp. 1–5, IEEE, Apr. 2019.

[22] Yang Song, Songlin Sun, Xiaojun Jing, and Hai Huang, "Orthogonality analysis and improvement of MSE-OFDM system," in *2010 International Conference on Information, Net-*

working and Automation (ICINA), (Kunming, China), pp. V1–433–V1–437, IEEE, Oct. 2010.

[23] Chiwoo Lim, Youngbin Chang, Jaeweon Cho, Panyuh Joo, and Hyeonwoo Lee, "Novel OFDM transmission scheme to overcome caused by multipath delay longer than cyclic prefix," in *2005 IEEE 61st Vehicular Technology Conference*, vol. 3, pp. 1763–1767 Vol. 3, May 2005.

[24] "LTE-chapter2-38to42.pdf." `https://m.eet.com/media/1072709/LTE_Chapter2_38to42.pdf`.

[25] H. Yin and S. Alamouti, "OFDMA: A Broadband Wireless Access Technology," in *2006 IEEE Sarnoff Symposium*, pp. 1–4, Mar. 2006.

[26] R. Prasad, *OFDM for wireless communications systems*. Artech House universal personal communications series, Boston, Mass.: Artech House, 2004. OCLC: 249829131.

[27] J. Zhang, L.-L. Yang, L. Hanzo, and H. Gharavi, "Advances in Cooperative Single-Carrier FDMA Communications: Beyond LTE-Advanced," *IEEE Communications Surveys & Tutorials*, vol. 17, no. 2, pp. 730–756, 2015.

[28] I. Al-Nahhal, M. Alghoniemy, A. B. Abd El-Rahman, and Z. Kawasaki, "Modified zero forcing decoder for ill-conditioned channels," in *2013 IFIP Wireless Days (WD)*, (Valencia, Spain), pp. 1–3, IEEE, Nov. 2013.

[29] K. Pachori and A. Mishra, "Performance analysis of MIMO systems under multipath fading channels using linear equalization techniques," in *2015 International Conference on Advances in Computing, Communications and Informatics (ICACCI)*, pp. 190–193, Aug. 2015. ISSN: null.

[30] N. S. Randhawa, S. Sharma, and R. K. Dubey, "A survey of equalization techniques for an effective equalizer design in MIMO-OFDM systems," in *2015 International Conference on Circuits, Power and Computing Technologies [ICCPCT-2015]*, pp. 1–5, Mar. 2015.

[31] I. Ahamed and M. Vijay, "Comparison of different diversity techniques in MIMO antennas," in *2017 2nd International Conference on Communication and Electronics Systems (ICCES)*, (Coimbatore), pp. 47–50, IEEE, Oct. 2017.

[32] L. Hanzo, H. Haas, S. Imre, D. O'Brien, M. Rupp, and L. Gyongyosi, "Wireless Myths, Realities, and Futures: From 3g/4g to Optical and Quantum Wireless," *Proceedings of the IEEE*, vol. 100, pp. 1853–1888, May 2012.

[33] S. A. Busari, K. M. S. Huq, S. Mumtaz, L. Dai, and J. Rodriguez, "Millimeter-Wave Massive MIMO Communication for Future Wireless Systems: A Survey," *IEEE Communications Surveys & Tutorials*, vol. 20, no. 2, pp. 836–869, 2018.

[34] S. Alamouti, "A simple transmit diversity technique for wireless communications," *IEEE Journal on Selected Areas in Communications*, vol. 16, pp. 1451–1458, Oct. 1998.

[35] G. J. Foschini, "Layered space-time architecture for wireless communication in a fading environment when using multi-element antennas," *Bell Labs Technical Journal*, vol. 1, pp. 41–59, Aug. 2002.

[36] "Amplifier Classes and the Classification of Amplifiers." `https://www.electronics-tutorials.ws/amplifier/amplifier-classes.html`, July 2013.

[37] P. K. Singya, N. Kumar, and V. Bhatia, "Mitigating NLD for Wireless Networks: Effect of Nonlinear Power Amplifiers on Future Wireless Communication Networks," *IEEE Microwave Magazine*, vol. 18, pp. 73–90, July 2017.

[38] J. C. Pedro and S. A. Maas, "A comparative overview of microwave and wireless power-amplifier behavioral modeling approaches," *IEEE Transactions on Microwave Theory and Techniques*, vol. 53, pp. 1150–1163, Apr. 2005.

[39] J. Weekley and B. Mangus, "TWTA versus SSPA: a comparison of on-orbit reliability data," *IEEE Transactions on Electron Devices*, vol. 52, pp. 650–652, May 2005.

[40] L. C. Nunes, P. M. Cabral, and J. C. Pedro, "AM/AM and AM/PM Distortion Generation Mechanisms in Si LDMOS and GaN HEMT Based RF Power Amplifiers," *IEEE Transactions on Microwave Theory and Techniques*, vol. 62, pp. 799–809, Apr. 2014.

[41] C. Rapp, "Effects of HPA nonlinearity on 4-DPSK/OFDM-signal for a digital sound broadcasting system," in *2nd Conference on Sattelite Communications*, (Liege, Belgium), Oct. 1991.

[42] J. Liebetreu, "Proposed System Impairment Models." `http://www.ieee802.org/16/tg1/phy/pres/802161pp-00_15.pdf`.

[43] Gang Tong, Qiang Wang, and Guixin Wang, "A performance controllable PA linearization scheme of joint PAPR reduction and predistortion," in *2012 IEEE 14th International Conference on Communication Technology*, pp. 1177–1181, Nov. 2012.

[44] F. Gregorio, S. Werner, T. I. Laakso, and J. Cousseau, "Receiver Cancellation Technique for Nonlinear Power Amplifier Distortion in SDMA–OFDM Systems," *IEEE Transactions on Vehicular Technology*, vol. 56, pp. 2499–2516, Sept. 2007.

[45] J. Tellado, L. M. C. Hoo, and J. M. Cioffi, "Maximum-likelihood detection of nonlinearly distorted multicarrier symbols by iterative decoding," *IEEE Transactions on Communications*, vol. 51, pp. 218–228, Feb. 2003.

[46] A. Silva, J. Assunção, R. Dinis, and A. Gameiro, "Performance evaluation of IB-DFE-based strategies for SC-FDMA systems," *EURASIP Journal on Wireless Communications and Networking*, vol. 2013, p. 292, Dec. 2013.

[47] X. Wang, L. Kong, F. Kong, F. Qiu, M. Xia, S. Arnon, and G. Chen, "Millimeter Wave Communication: A Comprehensive Survey," *IEEE Communications Surveys Tutorials*, vol. 20, no. 3, pp. 1616–1653, 2018.

[48] "(PDF) Millimeter wave FMCW radar for Foreign object debris (FOD) detection at airport runways." `https://www.researchgate.net/publication/237149851_Millimeter_wave_FMCW_radar_for_Foreign_object_debris_FOD_detection_at_airport_runways`.

[49] T. Nitsche, C. Cordeiro, A. B. Flores, E. W. Knightly, E. Perahia, and J. C. Widmer, "IEEE 802.11ad: directional 60 GHz communication for multi-Gigabit-per-second Wi-Fi [Invited Paper]," *IEEE Communications Magazine*, vol. 52, pp. 132–141, Dec. 2014.

[50] T. Baykas, C.-S. Sum, Z. Lan, J. Wang, M. A. Rahman, H. Harada, and S. Kato, "IEEE 802.15.3c: the first IEEE wireless standard for data rates over 1 Gb/s," *IEEE Communications Magazine*, vol. 49, pp. 114–121, July 2011.

[51] S. Rangan, T. S. Rappaport, and E. Erkip, "Millimeter-Wave Cellular Wireless Networks: Potentials and Challenges," *Proceedings of the IEEE*, vol. 102, pp. 366–385, Mar. 2014.

[52] Z. Pi and F. Khan, "An introduction to millimeter-wave mobile broadband systems," *IEEE Communications Magazine*, vol. 49, pp. 101–107, June 2011.

[53] H. Q. Ngo, E. G. Larsson, and T. L. Marzetta, "Energy and Spectral Efficiency of Very Large Multiuser MIMO Systems," *IEEE Transactions on Communications*, vol. 61, pp. 1436–1449, Apr. 2013.

[54] K. Zheng, S. Ou, and X. Yin, "Massive MIMO Channel Models: A Survey," 2014.

[55] A. L. Swindlehurst, E. Ayanoglu, P. Heydari, and F. Capolino, "Millimeter-wave massive MIMO: the next wireless revolution?," *IEEE Communications Magazine*, vol. 52, pp. 56–62, Sept. 2014.

[56] G. Americas, "White paper: Advanced antenna systems for 5g," p. 125.

[57] K. Zheng, L. Zhao, J. Mei, B. Shao, W. Xiang, and L. Hanzo, "Survey of Large-Scale MIMO Systems," *IEEE Communications Surveys & Tutorials*, vol. 17, no. 3, pp. 1738–1760, 2015.

[58] R. W. Heath, N. González-Prelcic, S. Rangan, W. Roh, and A. M. Sayeed, "An Overview of Signal Processing Techniques for Millimeter Wave MIMO Systems," *IEEE Journal of Selected Topics in Signal Processing*, vol. 10, pp. 436–453, Apr. 2016.

[59] J. Via, I. Santamaria, V. Elvira, and R. Eickhoff, "A General Criterion for Analog Tx-Rx Beamforming Under OFDM Transmissions," *IEEE Transactions on Signal Processing*, vol. 58, pp. 2155–2167, Apr. 2010.

[60] A. Alkhateeb, J. Mo, N. Gonzalez-Prelcic, and R. W. Heath, "MIMO Precoding and Combining Solutions for Millimeter-Wave Systems," *IEEE Communications Magazine*, vol. 52, pp. 122–131, Dec. 2014.

[61] F. Sohrabi and W. Yu, "Hybrid Analog and Digital Beamforming for mmWave OFDM Large-Scale Antenna Arrays," *IEEE Journal on Selected Areas in Communications*, vol. 35, pp. 1432–1443, July 2017.

[62] X. Song, T. Kuhne, and G. Caire, "Fully-Connected vs. Sub-Connected Hybrid Precoding Architectures for mmWave MU-MIMO," in *ICC 2019 - 2019 IEEE International Conference on Communications (ICC)*, pp. 1–7, May 2019. ISSN: 1550-3607.

[63] R. Magueta, S. Teodoro, D. Castanheira, A. Silva, R. Dinis, and A. Gameiro, "Multiuser Equalizer for Hybrid Massive MIMO mmWave CE-OFDM Systems," *Applied Sciences*, vol. 9, p. 3363, Jan. 2019.

[64] J. Du, W. Xu, H. Shen, X. Dong, and C. Zhao, "Hybrid Precoding Architecture for Massive Multiuser MIMO With Dissipation: Sub-Connected or Fully Connected Structures?," *IEEE Transactions on Wireless Communications*, vol. 17, pp. 5465–5479, Aug. 2018.

[65] N. Ermolova and S.-G. Haggman, "An extension of Bussgang's theory to complex-valued signals," in *Proceedings of the 6th Nordic Signal Processing Symposium, 2004. NORSIG 2004.*, pp. 45–48, June 2004.

[66] H. E. Rowe, "Memoryless nonlinearities with Gaussian inputs: Elementary results," *The Bell System Technical Journal*, vol. 61, pp. 1519–1525, Sept. 1982.